THE DEVELOPMENT OF THE PENINSULA BLISTER FRACTURE TEST FOR ADHESIVELY BONDED JOINTS

by

Yong Bao

Submitted in partial fulfillment of the requirements for the degree of

MASTER OF SCIENCE

in

Engineering Mechanics

at

Virginia Polytechnic Institute and State University

Approved by:

David A Dillard

Dr. D. A. Dillard, Chairman

O. H. Griffin

Dr. O. H. Griffin

J. P. Wightman

Dr. J. P. Wightman

May, 1992

Blacksburg, Virginia

THE DEVELOPMENT OF THE PENINSULA BLISTER FRACTURE TEST FOR ADHESIVELY BONDED JOINTS

by

Yong Bao

Submitted to the Department of Engineering Science and Mechanics
in partial fulfillment of the requirements for the degree of
Master of Science in Engineering Mechanics

ABSTRACT

This study reports on the development and application of the peninsula blister test to quantitatively measure the adhesion of various adhesively bonded joints. Analytical results reveal that this peninsula-like geometry benefits from both a constant strain energy release rate over the major portion of the debond length and a high strain energy release rate at any given pressure. Applications of this technique to several adhesion systems were conducted. Although some of these systems haven't been successfully tested due to various reasons, experimental results from systems of PSA tapes and thin polyimide films bonded on aluminum substrates were promising. The agreement of the bond strength in terms of strain energy release rates obtained from both experimental and analytical methods from the last two systems indicates the feasibility of this technique. Primary studies on the stress analysis for several thin film adhesion tests suggest that the high ratio of strain energy release rate to applied pressure offered by this modified blister geometry may not be

able to overcome the tensile strength limitations of thin film adhesion testing. Further studies need to be conducted in order to understand if the strain energy release rate can be raised without the increase of membrane stresses by altering specimen geometries. In conclusion, although this modified blister is not an universal adhesion test for every adhesion system, the attractive nature of the constant strain energy release rate produced by the peninsula blister specimen warrants further investigations and wider applications.

ACKNOWLEDGMENT

Many sincere thanks go to my thesis advisor, Dr. David A. Dillard, for providing me the opportunity to investigate this project. His professional guidance and wise insights throughout my graduate program are gratefully acknowledged. I also extend appreciation to Dr. James P. Wightman and Dr. Griffin, for their helpful comments and serving as my committee members.

The financial support provided by the National Science Foundation's "High Performance Polymeric Adhesives and Composites" Science and Technology Center at VPI & SU is gratefully acknowledged.

I would like to express my thanks to all the folks in Adhesion Lab, Yeou-Shin Chang, Yeh-Hung Lai, Jack Lesko, Dwayne Rakestraw, Hari Reddy, and John Wang, who have influenced, instructed and supported me in various ways. My thanks also go to Mr. Danny Reed, for assisting with specimen machining, and to Francis Webster, for helping with making the specimens and the control systems. A special thanks goes to my buddy in Blacksburg, Katherine Wu, for her friendship and the prayers throughout my studies here.

I owe my deepest gratitudes to my husband and best friend, Yutong Wu, for spending these two and half years alone far away in New Jersey. The completion of this thesis would have been impossible without his understanding and continuous encouragement. My foremost thanks go to my parents and my sisters, for their endless love and support during my pursuit of education in United States, as well as in China.

TABLE OF CONTENTS

LIST OF FIGURES

LIST OF TABLES

CHAPTER 1. INTRODUCTION

1.1 INTRODUCTION OF VARIOUS ADHESION TESTS

Adhesive applications have increased rapidly due to advances in adhesive materials and improvements of bonding techniques over the last few decades. Correspondingly, adhesion strength measurement is becoming increasingly important. In almost all adhesively bonded systems, bond strength plays a very important role in the performance and reliability of the whole system. Many examples can be given to illustrate the need for a reliable and reproducible adhesion test. A good adhesion test should not only be able to compare the effects of different factors, such as surface preparation, curing methods, and bonding technique, on bond strength, but also be able to quantitatively evaluate the bond strength of the adhesively bonded systems. As Lord Kelvin stated in the mid-nineteenth century, "Until we can quantify and express something in numbers, our knowledge of it is meager."

A number of fracture tests have been proposed to evaluate the bond strength of adhesively bonded systems. No universal technique is available for all adhesively bonded systems because each test has its own unique merits and drawbacks. The results of some are easily analyzed but require costly machining and fabrication while others are simple to prepare but require complicated analysis. In this chapter, a brief review will be made of some

testing techniques presently being used with an emphasis on blister tests, followed by a scope of research.

Prior to the introduction of various adhesion tests, it should be emphasized that one of the most important concepts in evaluating the strength of an adhesively bonded system is the strain energy release rate, G, which is also termed the fracture energy or debond energy. Many attempts have been made to develop testing techniques which can produce constant strain energy release rates during crack propagation by modifications of specimen geometries or loading methods. The significance of a constant strain energy release rate for testing adhesively bonded joints will also be discussed in this chapter.

When both of the adherend materials are relatively stiff, a number of fracture tests may be used. The double cantilever beam (DCB) specimen was first proposed by Obreimoff [1] in 1930 in testing crack propagation of monolithic materials, and was adapted to adhesively bonded joints by Mostovoy and Ripling [2] in the 1960s for testing Mode I fracture behavior. According to Mostovoy and Ripling, the strain energy release rate for a typical DCB specimen shown in Figure 1.1(a) can be expressed as:

$$G=\frac{12P^2a^2}{Eh^3b^2} \quad (1.1)$$

where, P represents the force acting perpendicular to the bond line, a represents the crack length, h represents the thickness of the adherends, b

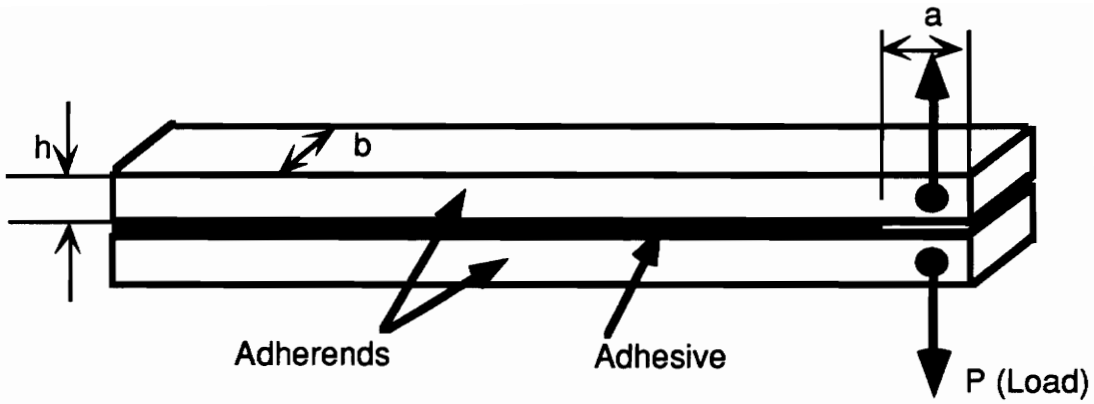

(a) Double cantilever beam (DCB) Specimen

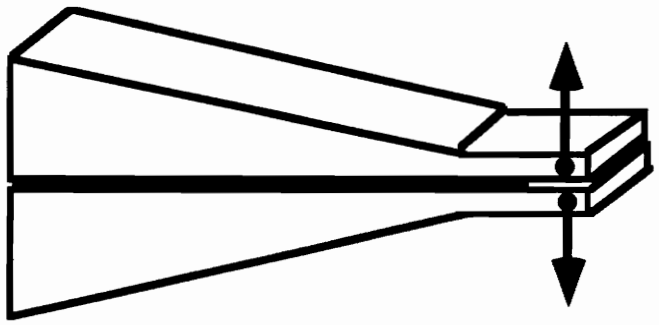

(b) Tapered double cantilever beam (TDCB) specimen

Figure 1.1. Double Cantilever Beam Specimens

represents the width of the adherend and the bond area, and E represents the Young's Modulus of the adherends.

From this equation, one may see that the prediction of the strain energy release rate for the DCB specimen involves many variables, including the joint geometry (b, h), the adherend material property (E), the applied load (P) and the crack length (a). It will be beneficial if attempts can be made to limit the number of variables to be monitored in an adhesion test. Equation (1.1) also indicates that the strain energy release rate (G) of the specimen is proportional to the square of the crack length (a) at a constant load (P). Therefore, after starting at the initial crack length, crack propagation becomes unstable under a constant load.

In order to obtain a constant strain energy release rate at a constant load, the tapered double cantilever beam (TDCB) specimen [3] was proposed. In this TDCB specimen, either the adherend thickness (h) or the adherend width (b) was designed to vary along the length of the specimen so that the term $\frac{a^2}{h^3}$ or $(\frac{a}{b})^2$in equation (1.1) is constant and a constant strain energy release rate can be produced. Figure 1.1(b) is a TDCB specimen that has a constant $\frac{a^2}{h^3}$ ratio lengthwise.

In such a constant strain energy release rate test, more data points can be collected in a single loading test because G is constant and independent of crack length under a constant load. Other advantages include less variables to

be monitored and stable debonding. In cases where crack length is not easy to measure, for instance, for fatigue tests, durability tests or for cases where the specimens have to be tested in an environmental chamber, a constant strain energy release rate test offers significant advantages.

Other fracture test specimens for stiff adherends include the single lap shear specimen and cone specimen advocated by Anderson and his associates [4], the blister specimen utilized by Anderson, et. al. [4], the double torsion specimen proposed by Outwater and Gerry [5], the cracked lap shear specimen investigated by Brussat [6], and the DCB specimen with a modified loading method developed by Dillard et. al. [7]. Among these tests, the last three offer constant strain energy release rates.

When at least one of the adherends of an adhesively bonded joint is a thin and flexible film, such as a pressure sensitive adhesive (PSA) tape, several techniques are available. The most popular test used in industry is the peel test [8-11]. Figure 1.2 shows both a typical peel geometry with take-off angle θ and a T-peel test geometry. Kaelble [8] analyzed the complicated stress state in a peel specimen. Gent [9] introduced the concepts of fracture mechanics into the peel specimen and studied the behavior of pressure sensitive adhesives with this test. Although the peel test is a versatile test and is very easy to perform, it suffers from the large bending and plastic deformation induced at large take-off angles. Thus, the analysis and interpretation of the test results are very difficult except under certain conditions. Small angle peel could reduce bending effects [8, 10], but some peel testers don't have small angle

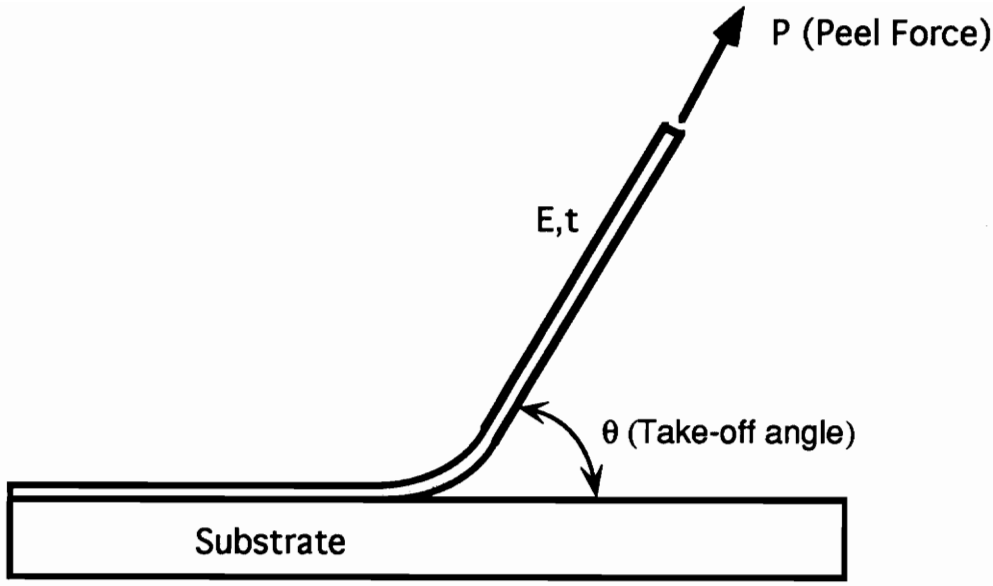

(b) Peel Specimen

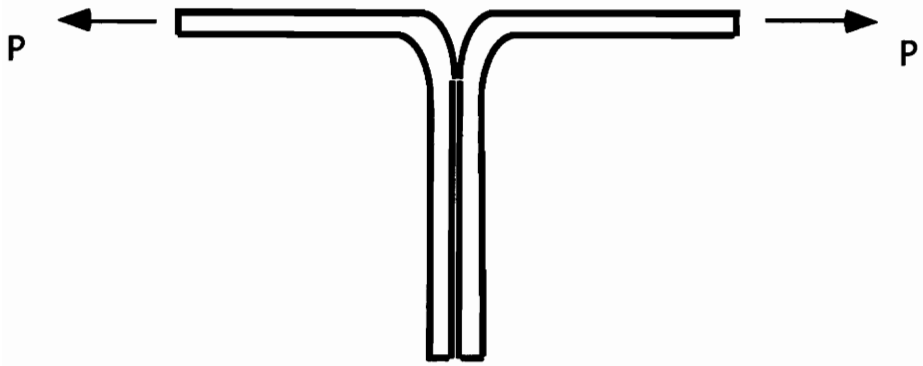

(c) T Peel Specimen

Figure 1.2 Peel Test Specimens

options. In spite of the problems associated with the peel specimens, various peel tests are still widely used by researchers and manufacturers to compare relative joint strengths or to study the effects of various surface preparations due to its simple geometry and testing procedures.

Another interesting group of adhesion tests that is often applied in measuring thin film adhesion is blister tests. The blister test was originally proposed by Dannenberg [11] in 1959 for measuring the adhesion of paints and varnishes. To have better control over the debonding growth, he confined the blister to form in a narrow groove, thereby resulting in a constant strain energy release rate specimen.

Williams [12] utilized a circular debond to measure the fracture energy of elastomeric materials adhesively bonded to a rigid substrate, which is termed the standard blister test in this research. Basically, the standard blister specimen consists of a top adherend bonded onto a rigid substrate with a central hole, shown in Figure 1.3. When a pressure (either pneumatic or hydraulic) is introduced into the center hole, the top adherend flexes and forms a blister. When the pressure reaches a critical value, the radius of the blister increases as debonding occurs between the top adherend and the substrate.

The blister test has several advantages over the peel test. First, debonding of blister specimen is usually accomplished by pneumatic or hydraulic pressures, therefore resulting in comparatively uniform stress distributions in film

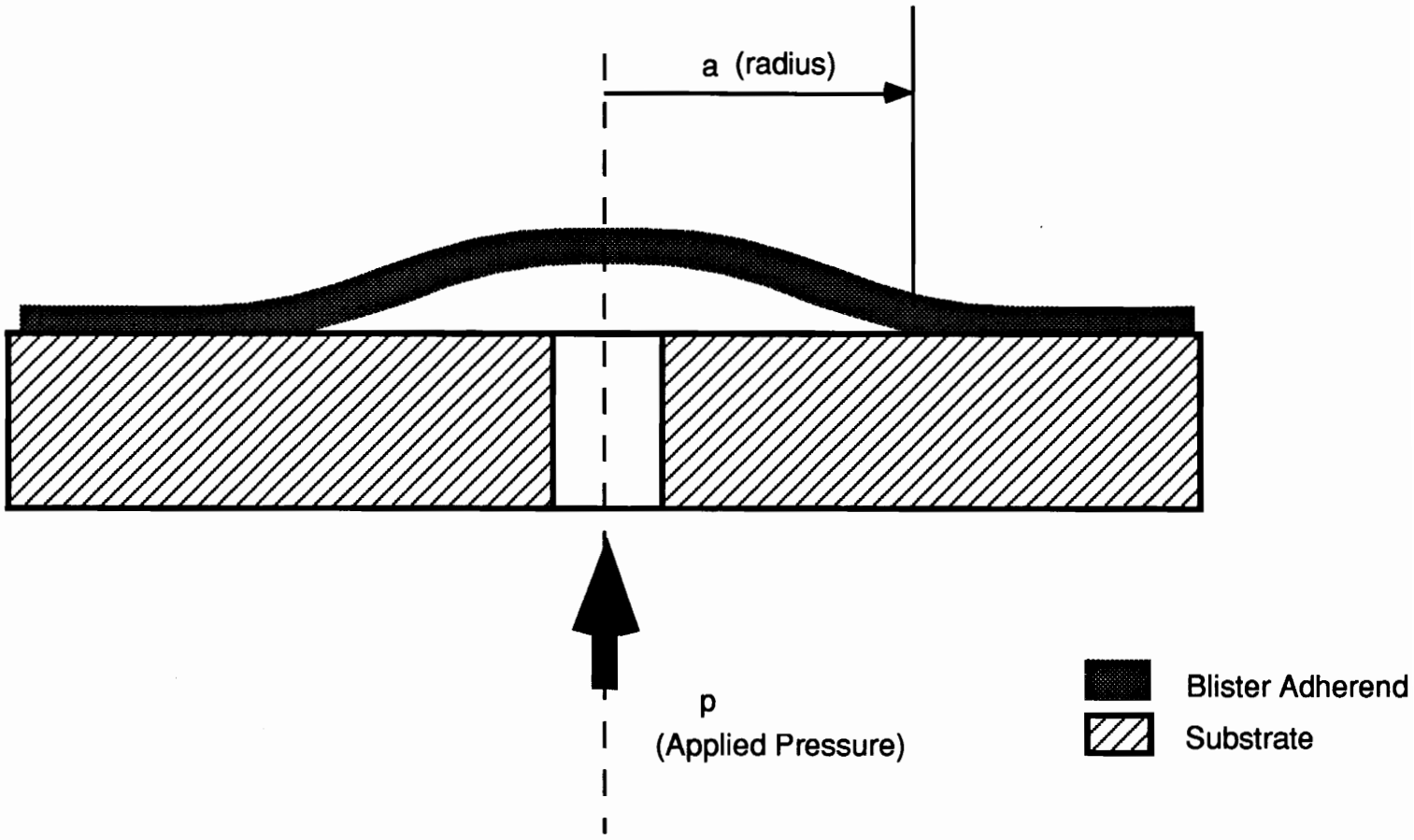

Figure 1.3 Standard Blister Specimen

adherends [28]. Second, the blister specimen is quite compatible with environmental exposures because the pressurizing medium is contained within the blister region. For circular versions of the blister specimen, the axisymmetric shape minimizes problems associated with the edge effects of finite width specimen, and diffusion perpendicular to the debonding front eliminates spurious effects for environmental exposure. In addition, since the peel angle in the blister test is small, it is expected that the effects of bending of the top adherend will be reduced. Owing to these advantages, blister tests have been applied to a wide variety of adhesion systems, including paints [11], pressure sensitive adhesive tapes [13], polymer coatings [11, 14], elastomers [12], bonded plates [15], and even the adhesion to ice [16].

However, there are still some problems associated with blister tests. According to Anderson, et al.[4], if the blister adherend is very stiff and can be taken as a thin plate, the strain energy release rate for a standard blister specimen illustrated in Figure 1.3 can be expressed as:

$$G=\frac{3(1-\nu^2)}{32Et^3}\cdot p^2a^4 \qquad (1.2)$$

where, p represents the applied pressure, a represents the debond radius, t represents the thickness of the blister adherend, E represents the Young's modulus of the blister adherend, and ν represents the Poisson's ratio of the blister adherend..

It can be seen that the strain energy release rate (G) is proportional to the fourth power of the debond radius (a). Hence, under a constant pressure, debonding becomes unstable as the debond radius grows. Another shortcoming of the standard blister specimen is that in order to calculate the strain energy release rate, it is necessary to measure both the applied pressure (p) and the debond radius (a). Since G is strongly dependent on radius, a small error in the measurement of the debond radius (a) could cause significant errors in calculating G. Another disadvantage of the standard blister specimen is that blister does not remain circular, which complicates the measurement of radius (a), and introduces errors in calculations.

Gent and Lewandowski [13] analyzed the standard blister specimen for the case of a very thin and flexible blister adherend that can be approximated as a membrane. In this case, the blister deformations are larger than the adherend thickness, and the bending effect can be neglected. The strain energy release rate is found to be:

$$G=\frac{5}{8}\left[\frac{3(1-\nu)}{8Et}\right]^{\frac{1}{3}}\cdot(pa)^{\frac{4}{3}} \qquad (1.3)$$

For these membrane specimens, the debond radius is not difficult to obtain because the blister deformation is larger. However, from equation (1.3), one may see that G is still proportional to debond radius raised to the 4/3 power ($a^{\frac{4}{3}}$). Therefore, it still results in unstable debonding at constant pressures.

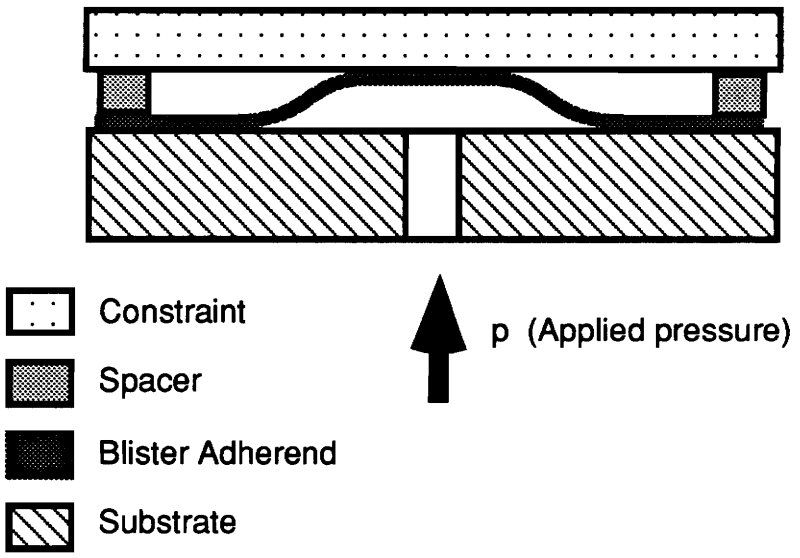

(a) Constrained Blister Specimen

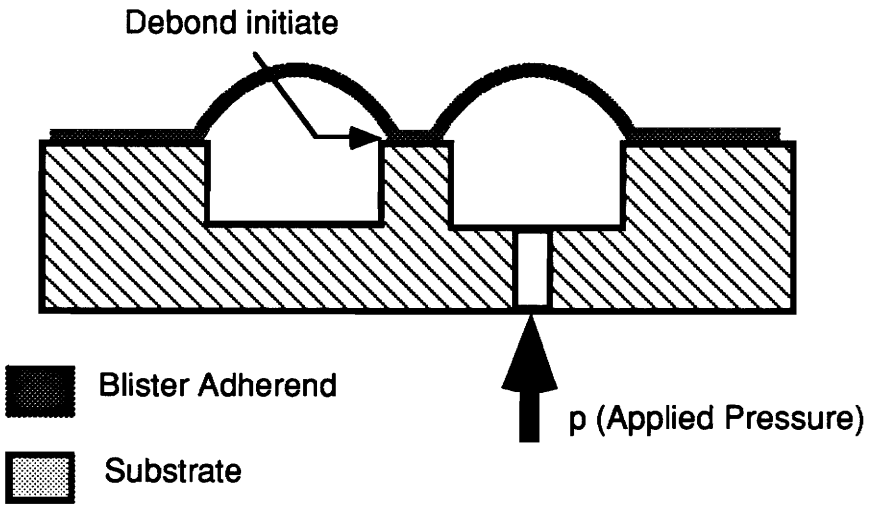

(b) Island Blister Specimen

Figure 1.4 Modified Blister Geometries

To minimize this unstable debonding problem, the constrained blister was introduced by Dillard et al.[15, 18] and Moet et al.[21], and analyzed by Lai and Dillard [18, 20]. The constrained blister geometry, as shown in Figure 1.4 (a), is easily formed by placing a rigid plate a small distance above the blister adherend. This plate is firmly held against a constant thickness spacer to keepit parallel with the substrate. As the blister grows, it comes in contact with the constraint and is prevented from further displacement. Because the work done is equal to the pressure times the volume displaced, and because a given blister element can only displace a distance equal to the constraint height, the constrained blister test approximates a constant strain energy release rate as the debond grows larger. The expression of the strain energy release rate for this blister geometry was found to be,

$$G = phq \qquad (1.4)$$

where, p is the applied pressure, h is the height of the constraint, and q is a correction factor. It has been shown experimentally by Chang et al. [15], that the correction factor q, which is a function of specimen geometry, ranged from 0.6 to 1 in the testing range. Thus this constrained blister specimen gives an almost constant strain energy release rate under a constant pressure and does significantly reduce the dependence of the strain energy release rate on the debond radius.

Nonetheless, the constrained blister specimen has encountered several problems. Questions have arisen regarding the effect of friction between the

adherend and the constraint. Although numerical results [18] suggest that the effect is totally negligible, the difficulty of analyzing a contact problem with such large deflections causes concern.

One common problem associated with the standard and the constrained blister test, as well as the peel test, is the tensile strength limitation. In other words, when testing thin film bonds with very strong adhesion, films may tear before debonding can be initiated. The island blister test, shown in Figure 1.4(b), was proposed by Senturia and Allen[21, 22] in order to overcome the tensile strength limitation of thin films. The island blister specimen derives the high ratio of strain energy release rate to applied pressure from the fact that the debonding front is reduced to a very small length. A small amount of debond propagation produces a relatively large increase in compliance, thereby giving rise to large strain energy release rates. When testing the adhesion of well-adhered thin film bonds with dominant prestress, it was found that debonding can be measured without film rupture by making the normalized island radius (b/a) small enough, where b is the island bond radius and a is the outside bond radius. The island blister specimen has been successfully applied to the adhesion measurements of polyimide film spin-coated on silicon wafers in microelectronic structures by Allen and Senturia. However, as will be shown later in Chapter 3.5, based on our recent analysis of the island blister test, the likelihood of film rupture cannot be overcome by the high ratio of strain energy release rates to applied pressure. Allen and Senturia's solutions are valid only in some limiting cases. Parenthetically, for an island blister geometry, when the membrane attachment site decreases in radius, the

calculated strain energy release rate increases without bound, thereby still results in unstable debonding.

In an attempt to keep the advantages and to overcome the limitations of the above blister tests, a geometric modification of the island blister specimen and Dannenburg's blister specimen, which was named the peninsula blister specimen, was proposed by Dillard and Bao [23]. In spite of some unresolved problems with this technique, as will be shown later, this interesting specimen could produce a truly constant strain energy release rate over a relatively large portion of the test specimen.

Most of the contents in Chapter 2 and Chapter 3 were published in the Journal of Adhesion in an article entitled "The Peninsula Blister Test: A High and Constant Strain Energy Release Rate Fracture Specimen for Adhesives" [24], where the introduction of the peninsula blister specimen and the solutions for plate and prestressed membrane cases were derived and written by Dr. David A. Dillard.

1.2 SCOPE OF RESEARCH

The objective of this research is to develop the peninsula blister test for evaluating the adhesion strength of adhesively bonded joints, especially for measuring the adhesion between thin films and rigid substrates. The development, analysis, and applications of the peninsula blister test to predict and measure the strain energy release rates of some adhesively bonded joints

are the major tasks of this research. The peninsula blister specimen will be introduced in Chapter 2. Theoretical solutions to predict the strain energy release rates for several cases will be shown in Chapter 3. Chapter 4 will detail the experimental apparatus and procedures. Chapter 5 will discuss the results of applying the peninsula blister test to several specific adhesive bond systems and comparing with other thin film testing techniques. A summary of this thesis and some recommendations for future efforts will be presented in Chapter 6.

CHAPTER 2. THE PENINSULA BLISTER SPECIMEN

As introduced in Chapter 1, the peninsula blister specimen is a natural extension of the island blister to a larger "geographical" feature [22]. The name coins from the fact that debonding occurs along a narrow "peninsula" which extends into the blister region, as shown in Figure 2.1. Being similar to the island blister specimen, the peninsula blister retains the advantageous high strain energy release rate for any given pressure. Unlike the island blister, the peninsula blister strain energy release rate does not increase without bound as the debond progresses, but results in the highly desirable constant strain energy release rate nature of the peninsula blister specimen. Added features of the peninsula blister geometry include the larger debonding areas and additional data points that can be obtained from a single specimen. Disadvantages are that the fabrication of the specimen may be difficult for certain material systems, and that the specimen is no longer axisymmetric, thereby possibly reducing the utility for environmental exposure testing. There is a mixture of mode I and II for the strain energy release rates; the nature of this mode mix has not yet been investigated.

In order to understand the fracture mechanics involved in these adhesion tests, it is instructive to recall that for fracture specimens that exhibit linear force versus deflection behavior, the strain energy release rate is obtained simply from:

$$G = \frac{1}{2} p^2 \frac{\partial C}{\partial A} \qquad (2.1)$$

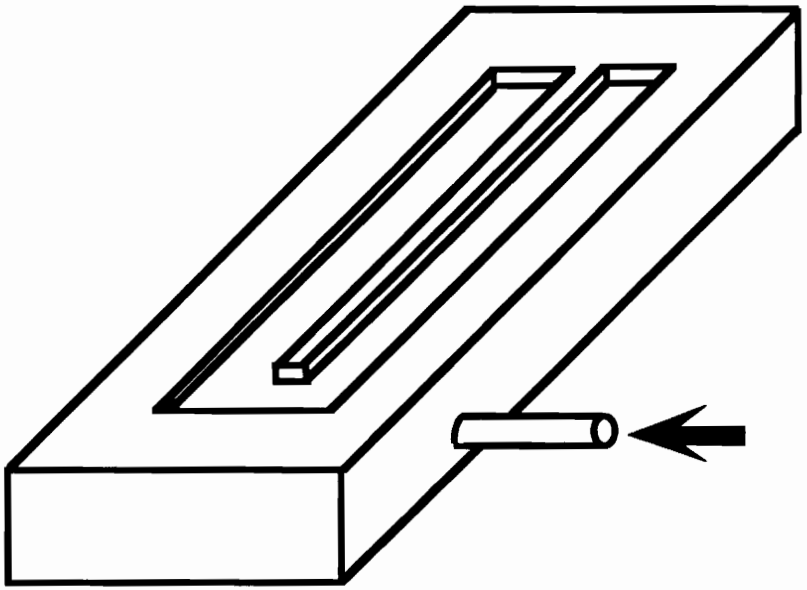

(a) Substrate for the peninsula blister

(b) Before debonding

(c) After debonding

Fig.2.1 Peninsula Blister Specimen

where p represents the generalized force (for pressurized blister geometries: pressure), C represents the generalized compliance (for blister: displaced volume/pressure), and A represents the debonded area

For a given pressure, the only two ways to increase G are to increase the increments in compliance produced by debonding, or to decrease the amount of debond area that is needed to produce a given amount of compliance. Each of these methods is frequently applied to various fracture geometries. For example, using more compliant adherends or longer initial debond increases the compliance change for double cantilever beam (DCB) specimens, whereas notching the beams to give reduced bond widths reduces the denominator in equation (2.1).

The island blister specimen may also be explained in terms of equation (2.1). It derives its high strain energy release rate from the fact that the debonding front is reduced to a very small length. Because the island blister specimen is axisymmetric, the change in area needed to affect a change in compliance becomes vanishingly small as the island bond radius (b) approaches zero. The volume changes do not vanish as the bond radius decreases, so unbounded strain energy release rates are possible for prestressed membrane specimens.

Analysis reveals that the strain energy release rates obtainable for a given pressure are very high for the peninsula blister. In fact, the peninsula blister often exceeds the very high values obtainable with the island blister. This may also be explained by equation (2.1). The high strain energy release rates for the peninsula blister specimen arise from two factors. The peninsula

width, 2b, is kept small to reduce the debonding area associated with a given increment in debonding length. More importantly, however, the specimen takes advantage of the tremendous changes in compliance which result as debonding proceeds along the peninsula. A comparison of the compliance changes for the island and peninsula blister geometries may be seen in Figure 2.2. Although direct comparison is not possible because the island specimen is axisymmetric and the peninsula is a linear geometry, it is seen that the compliance change of the latter can be much larger. The primary difference arises because the island blister ceases to be a fracture test once the island radius vanishes. A large compliance change occurs as the membrane displaces following complete debonding. However this large compliance change does not contribute to a fracture event. On the other hand, the peninsula blister is able to take advantage of this full compliance change as the debonding proceeds along the peninsula in a self-similar manner. This produces very large strain energy release rates for any given pressure.

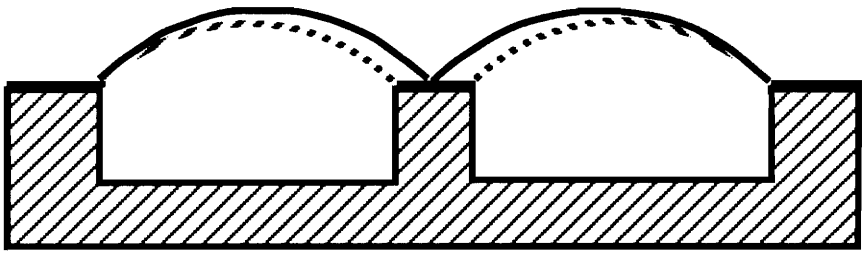

Compliance change for island blister specimen

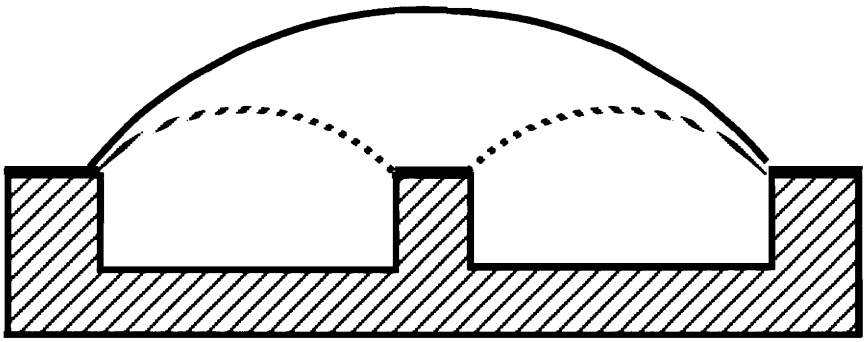

Compliance change for peninsula blister specimen

Figure 2.2 A Schematic Contrasting Compliance Changes with the Island and Peninsula Blister Specimen

CHAPTER 3. ANALYTICAL SOLUTIONS

Due to the complexity of geometry, it is very difficult to analytically model the peninsula blister specimens. The nature of the mode mix and the exact blister shapes around the debonding front haven't been determined in this study. However, due to the nature of self - similar debonding, strain energy release rates for the peninsula blister on a rigid substrate can be determined analytically. This chapter will present results for cases where the blister behaves as a plate, as a membrane with a dominant prestress, as a membrane with no prestress, and as a membrane with initial slack. These will be compared with solutions for other blister geometries. To simplify the analysis and without losing the practicality, we will assume that the length dimensions of the peninsula blister specimens are much larger than the width dimensions. We have shown for the plate case that this assumption can be fulfilled by convenient specimen geometries. In the last section of this chapter, studies have also been conducted to discuss the relations between the strain energy release rate and membrane stress for several thin film adhesion test geometries.

3.1 PLATE SOLUTION

If one assumes that the blister adherend has bending resistance, the total deflections of the blister do not exceed the order of the thickness of the blister

adherend, and the plate width is much larger than the thickness of the blister adherend, simple plate theory can be applied. The governing equation is

$$\nabla^4\omega=-\frac{p}{D} \qquad (3.1.1)$$

where, ∇^4 is the biharmonic operator, ω is the deflection of the plate, p is the applied pressure, and D is the plate rigidity given by

$$D = \frac{Et^3}{12(1 - \nu^2)} \qquad (3.1.2)$$

where, E is Young's Modulus of the plate adherend, t is the plate thickness, and ν is Poisson's ratio of the plate adherend.

For a fully clamped plate with infinite length, as indicated in Figure 3.1.1(a), the displacement across the width of the plate is easily shown to be

$$\omega(x) = \frac{px^2}{24D}(w-x)^2 \qquad (3.1.3)$$

where, w is the plate width, and p is a uniformly applied pressure.

The compliance per unit length is

$$\bar{C}=\frac{1}{p}\int_0^w \omega(x)dx=\frac{w^5}{720D} \qquad (3.1.4)$$

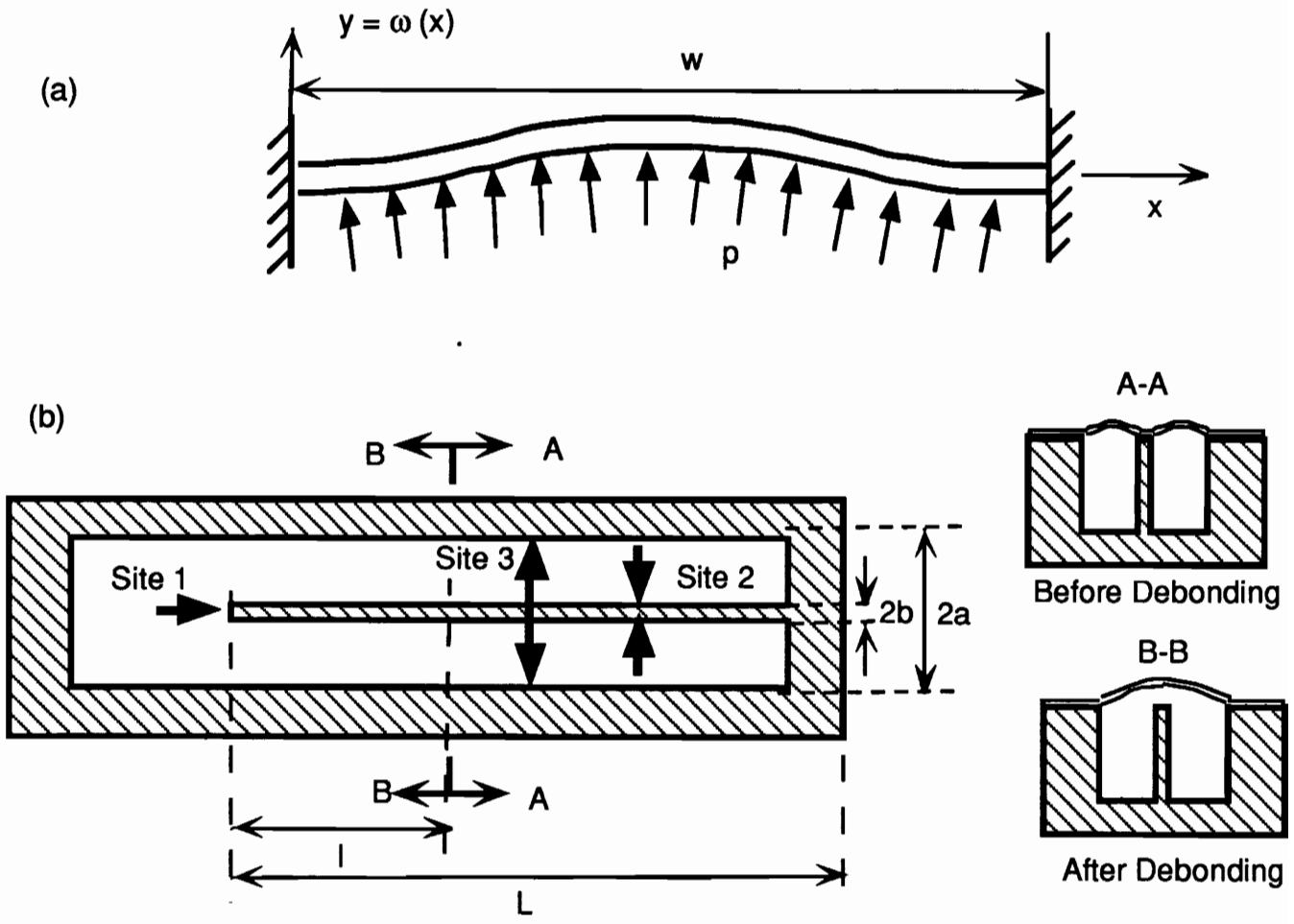

Fig. 3.1.1 Peninsula Blister Geometry (plate adherend)

Substituting (3.1.4) into (2.1), we find that the strain energy release rate to uniformly debond an infinitely long plate strip is:

$$G=\frac{p^2w^4}{288D} \qquad (3.1.5)$$

Thus for the peninsula blister specimen shown in Figure 3.1.1(b), we can write the strain energy release rate for debonding along sites 2 and 3 as:

$$G_2=\frac{p^2(a-b)^4}{288D} \qquad (3.1.6)$$

$$G_3=\frac{p^2a^4}{18D} \qquad (3.1.7)$$

For small b, G_2 may be approximated by

$$G_2=\frac{p^2a^4}{288D} \qquad (3.1.8)$$

From equation. (3.1.7) and (3.1.8), we can see that G_3 is at least 16 times the value of G_2.

From equation. (3.1.4), we note that, along the peninsula, the compliance per unit length before debonding is

$$\bar{C}_{bonded}=2\cdot\left[\frac{(a-b)^5}{720D}\right] \qquad (3.1.9)$$

and after debonding

$$\bar{C}_{debonded} = \frac{(2a)^5}{720D} \qquad (3.1.10)$$

Therefore, at a certain debonding length, we can write the total compliance of the specimen as,

$$C_{total} = l \cdot \bar{C}_{debonded} + (L - l) \cdot \bar{C}_{bonded} \qquad (3.1.11)$$

where, L is the total length of the peninsula, and l is the debonded peninsula length, as shown in Figure 3.1.1(b).

Substituting equation (3.1.11) into equation (2.1), the strain energy release rate along the peninsula. i.e. at site 1, can be obtained,

$$G_1 = \frac{p^2}{1440Db}\left[16a^5 - (a-b)^5\right] \qquad (3.1.12)$$

Because G_1 is larger than G_2 for all debonding lengths, debonding along the peninsula should always occur along the length rather than across the width. It is noted that for $b/a > 0.2$, debonding along site 3 is more likely than along site 1. This, however, can easily be avoided by clamping the perimeter of the specimen. As suggested in equation (3.1.12), however, to obtain larger strain energy release rates, the peninsula width (2b) should be less than 20% of the total specimen width (2a).

In Figure 3.1.2, the strain energy release rates normalized by p^2/D are plotted versus the normalized peninsula width for debonding along sites 1, 2, and 3. For comparison purposes, the island blister specimen with a plate adherend and similar cross sectional dimensions was analyzed using the numerical scheme developed by Lai and Dillard [18] and is also shown in Figure 3.1.2. Incidentally, a closed form plate solution for the island blister will be presented in Appendix A. To emphasize the variations of the strain energy release rates at small values of b/a, the same information as indicated in Figure 3.1.2 has been plotted in Figure 3.1.3 on logarithmic scales. These results reveal that for plate solution, peninsula blister specimens always produce larger values of G^*D/p^2 than island blister specimens with similar cross sectional dimensions. It should be noted that while the strain energy release rate for the peninsula blister is larger than the island blister with similar cross sectional dimensions, the peninsula blister is considerably longer. If the length of the peninsula blister was required to be the same as the island blister diameter, the island blister could give a higher strain energy release rate.

Before leaving the plate solution, it is instructive to see under what conditions the infinite solution proposed above becomes approximately valid for finite length plates. Based on the data in Timoshenko and Woinowsky-Krieger [26], the effect of aspect ratio l/a on the midpoint deflection for a fully clamped plate is illustrated in Figure 3.1.4. For example, with an aspect ratio of 2, the deviation from the infinite plate solution is only 2%. One can argue that if the aspect ratios of the end regions of the peninsula blister are greater than 2,

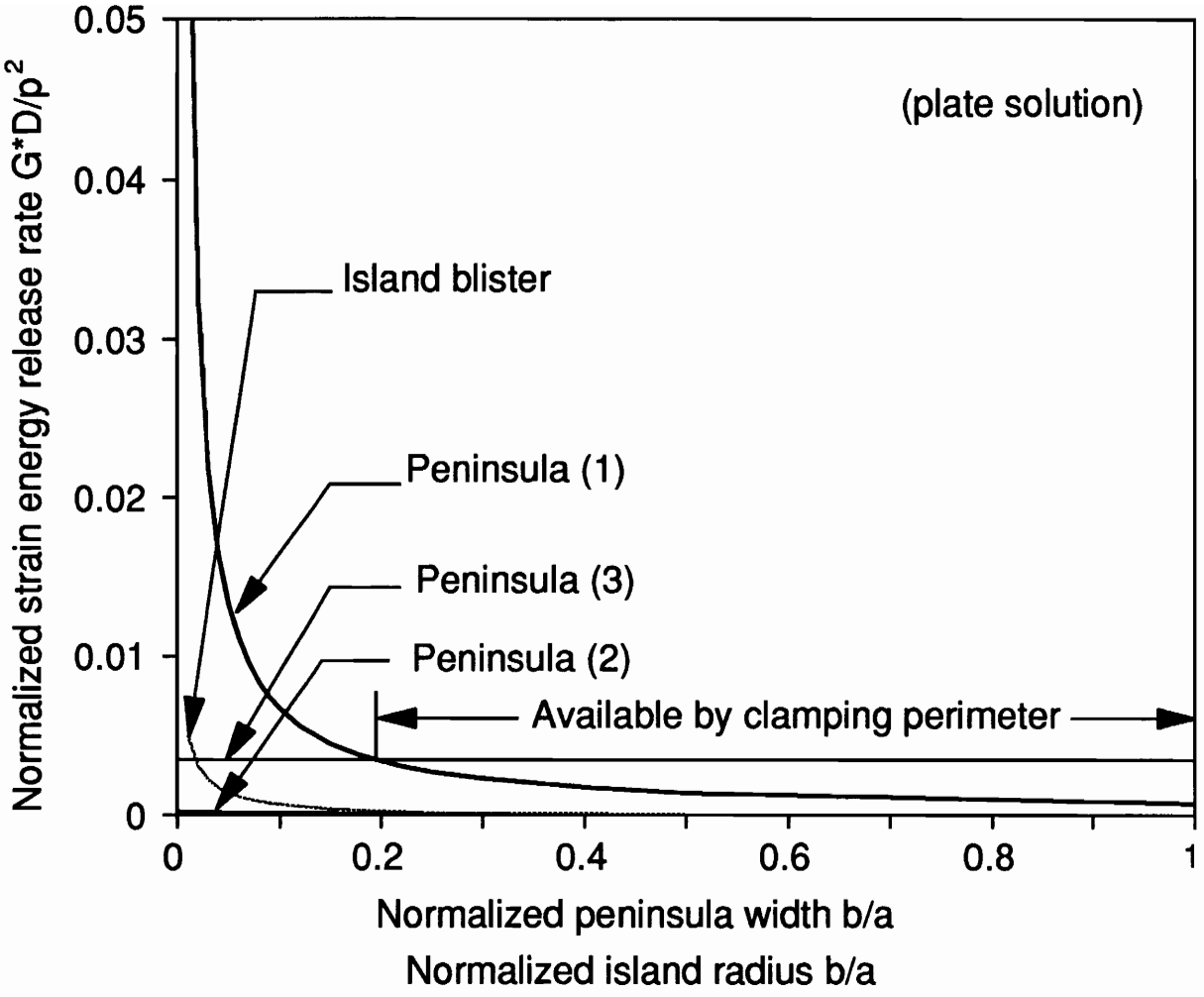

Figure 3.1.2 Effect of relative peninsula width on the strain energy release rate of the island and peninsula blister specimen

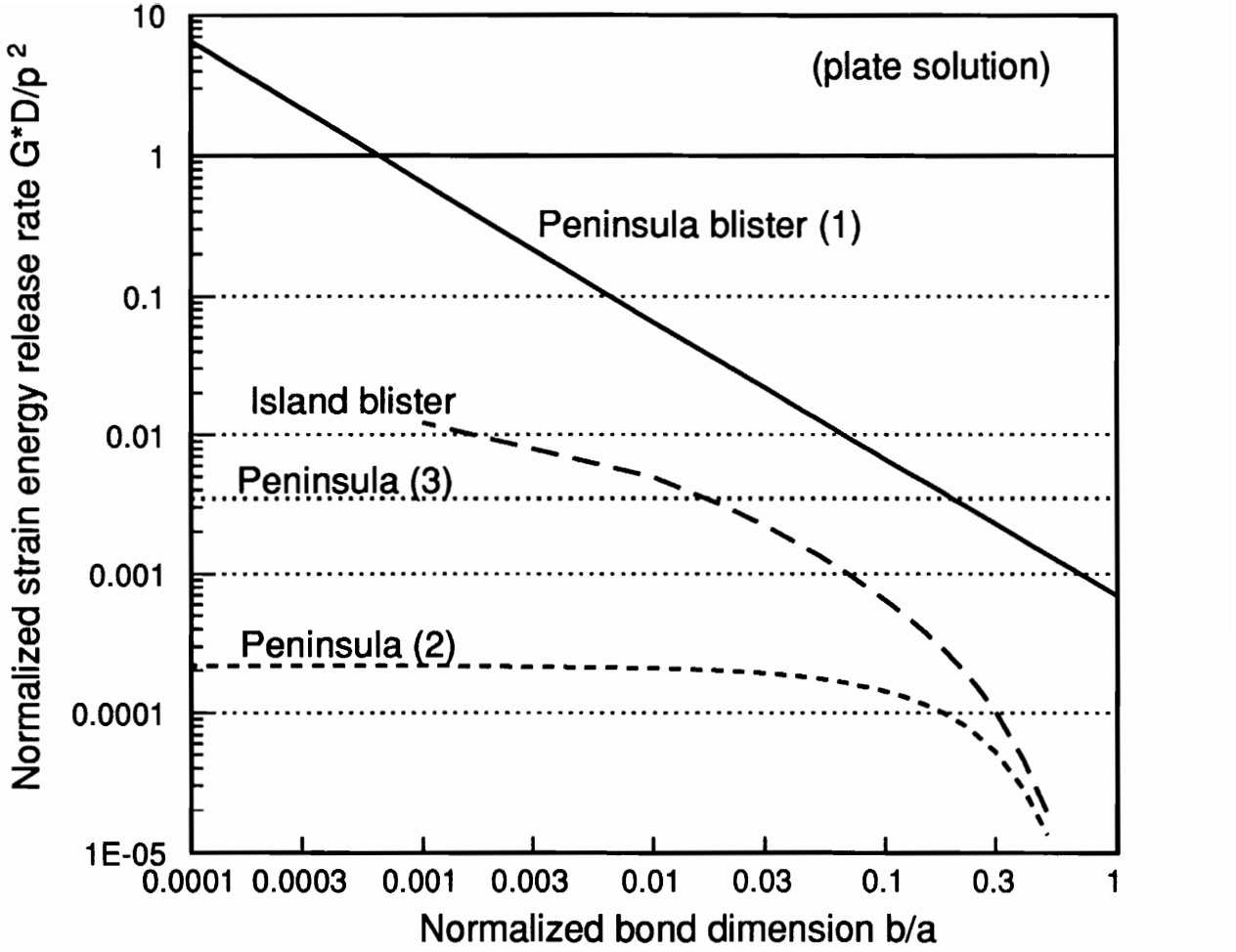

Figure 3.1.3 Effect of relative peninsula width on the strain energy release of the island and peninsula blister specimens

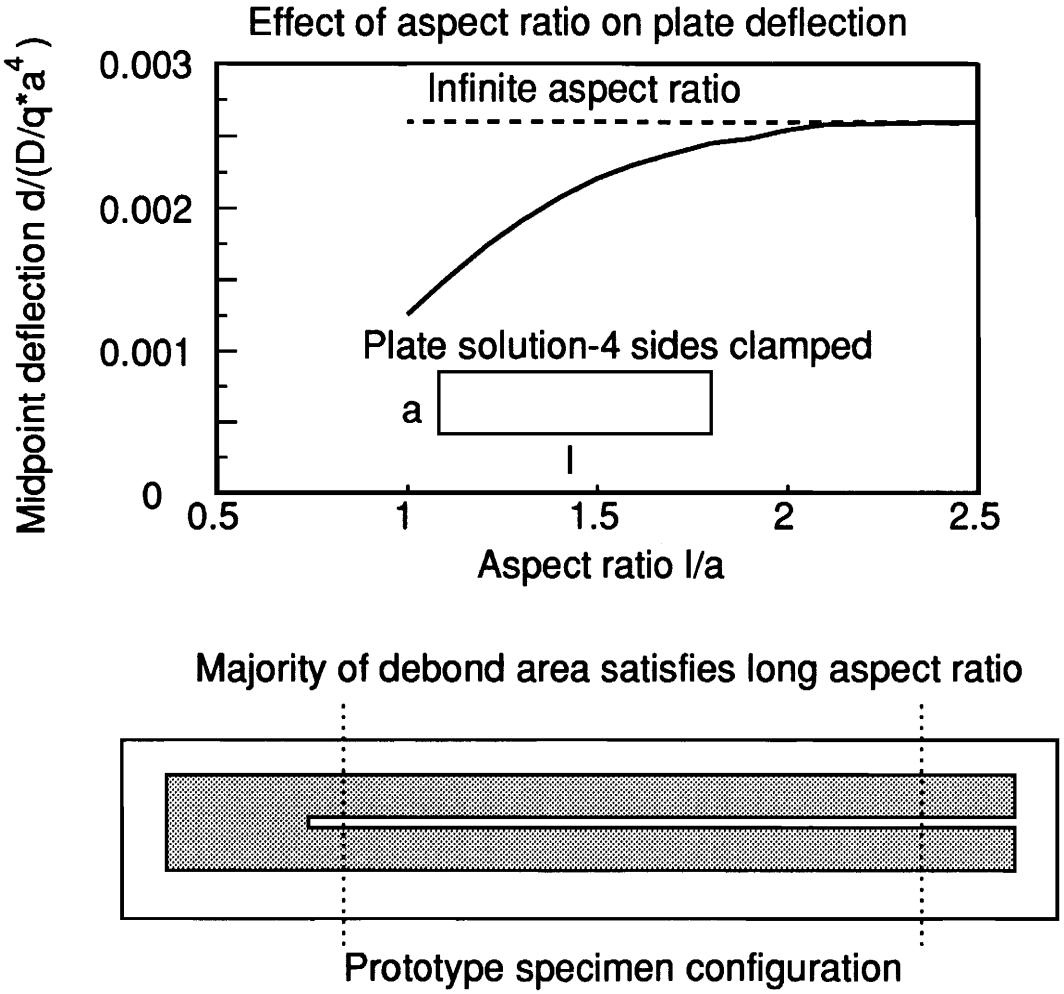

Figure 3.1.4 Influence of aspect ratio on the midpoint deflection of a rectangular plate and large central region of the prototype specimen with aspect ratios greater than 2

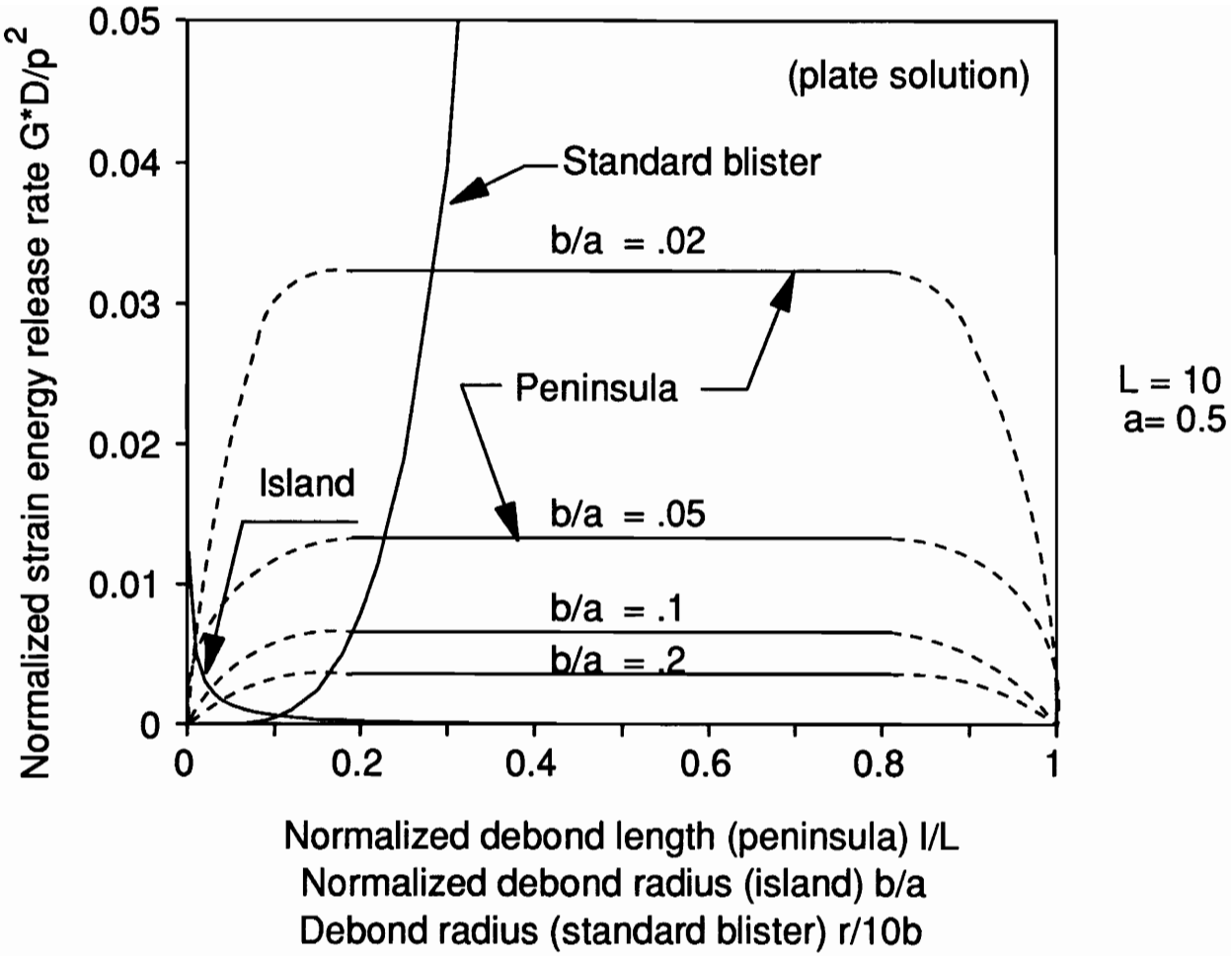

Figure 3.1.5 Variation in strain energy release rate with debond distance for the standard, island and peninsula blister specimens

deviations from the above solutions should be negligible. We, thus, neglect data obtained near the two ends of the peninsula, $l < 4a$ and $l > L-2(a-b)$. An optimum gap at the end of the peninsula tip is approximately 4a, although a small gap may be desirable for some materials to allow a debond to begin propagation outside of the test section. Deviations from constant strain energy release rate within the remainder of the specimen should be completely negligible. Based on this reasoning, Figure 3.1.5 compares the variations of the strain energy release rates for the standard, island, and peninsula blisters. The comparison suggests a significant advantage for the peninsula blister geometry because of the large test windows with constant strain energy release rate.

3.2 SOLUTIONS FOR MEMBRANE WITH DOMINANT PRESTRESS

When the adherend in a pressurized blister specimen is a flexible and thin film, it would be more appropriate to model such an adherend as a membrane rather than a plate. Membrane solutions are more difficult than plate solutions because the load-deflection behavior is nonlinear, in general. An exception to this is the case where the membrane is initially prestressed in tension, and the applied pressures and resulting deflections are small enough that the additional membrane stresses induced are negligible when compared to the initial prestress. This initial prestress may come from, for instance, residual stresses due to temperature changes during specimen fabrication, or intentionally applied stress. The governing differential equation is simply given by

$$\nabla^2\omega=-\frac{p}{N} \qquad (3.2.1)$$

where, N is the prestress in force per unit length. Interestingly, no material properties appear in this equation.

For the peninsula blister, the boundary conditions can be expressed as,

$$\omega(0) = \omega(w) = 0 \qquad (3.2.2)$$

By applying (3.2.2) and solving the differential equation (3.2.1), the deflection can be obtained as:

$$\omega(x)=-\frac{px^2}{2N}+\frac{pwx}{2N} \qquad (3.2.3)$$

where, x is the width direction, and y is the longitudinal direction. For long aspect ratios, the membrane tension in the y direction, N_y, does not affect the solution away from the ends. Therefore, the membrane tension, N, can be replaced by N_x, the membrane tension in the x direction.

Following a similar procedure as used in the plate solution, the compliance per unit length can be obtained:

$$\bar{C}=\frac{w^3}{12N_x} \qquad (3.2.4)$$

And the strain energy release rates for the three debonding sites can be determined as follows:

$$G_1=\frac{p^2}{24N_x b}\left[4a^3-(a-b)^3\right] \qquad (3.2.5)$$

$$G_2=\frac{p^2(a-b)^2}{8N_x} \qquad (3.2.6)$$

$$G_3=\frac{p^2a^2}{2N_x} \qquad (3.2.7)$$

Again we find that G_1 is always much larger than G_2, which reveals that debonding along the length of the peninsula is always favored over debonding across the width. It is also found that the debonding at site 1 is favored over site 3 for $b < 0.3\ a$. In actual application, to ensure the debonding occurs along the peninsula length (site 1), the periphery of the peninsula is clamped, therefore, debonding at site 3 may be prevented.

Allen and Senturia [23] have solved the problem of the membrane with prestress for the island blister, obtaining

$$G=\frac{p^2b^2}{32N}\left[\frac{(\beta^2-1)}{\ln\beta}-2\right]^2 \qquad (3.2.8)$$

where, $\beta=\frac{b}{a}$

The above results are shown in Figure. 3.2.1 and Figure 3.2.2. It is interesting to note that for similar a and b values, the strain energy release rate for the

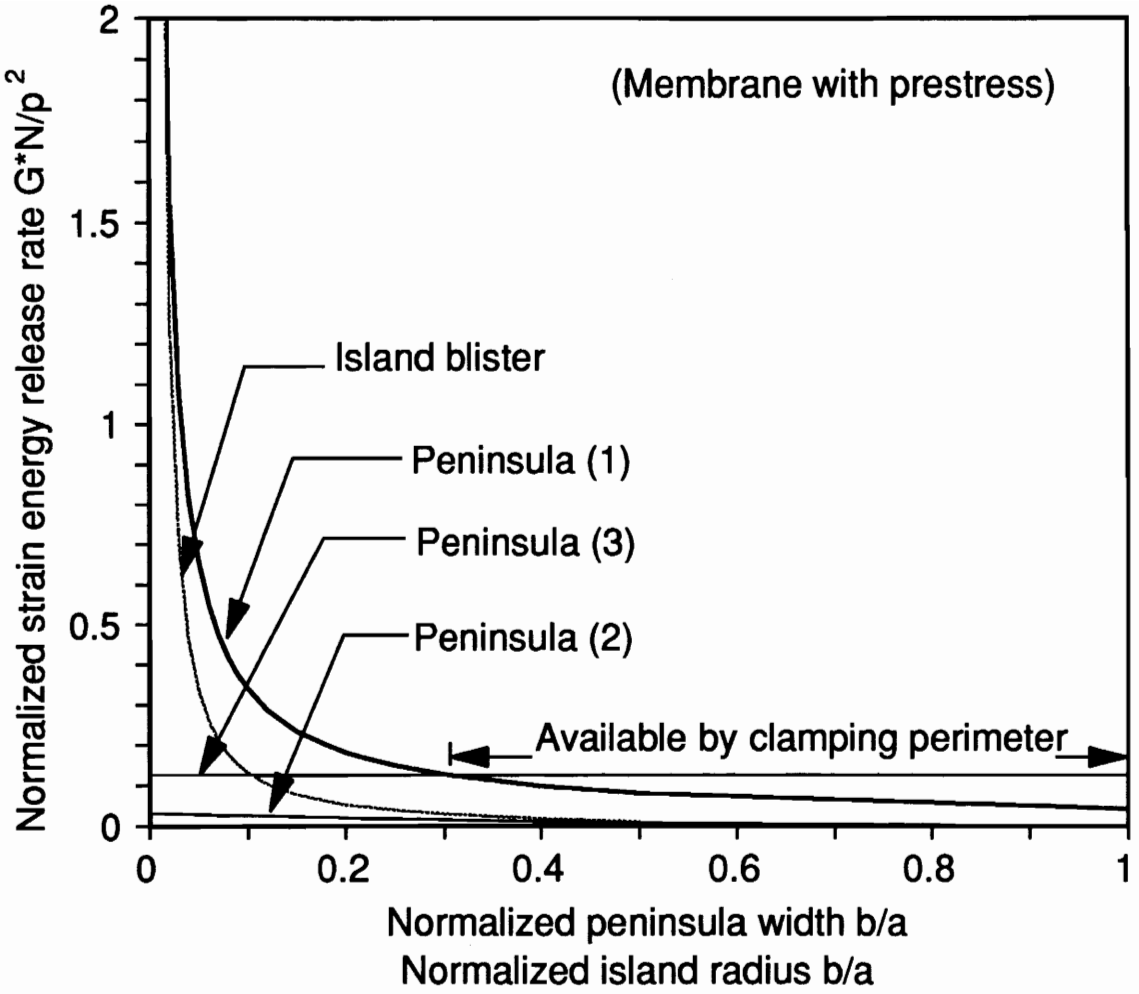

Fig. 3.2.1 Effect of relative peninsula width on the strain energy release rate of the island and peninsula blister specimens

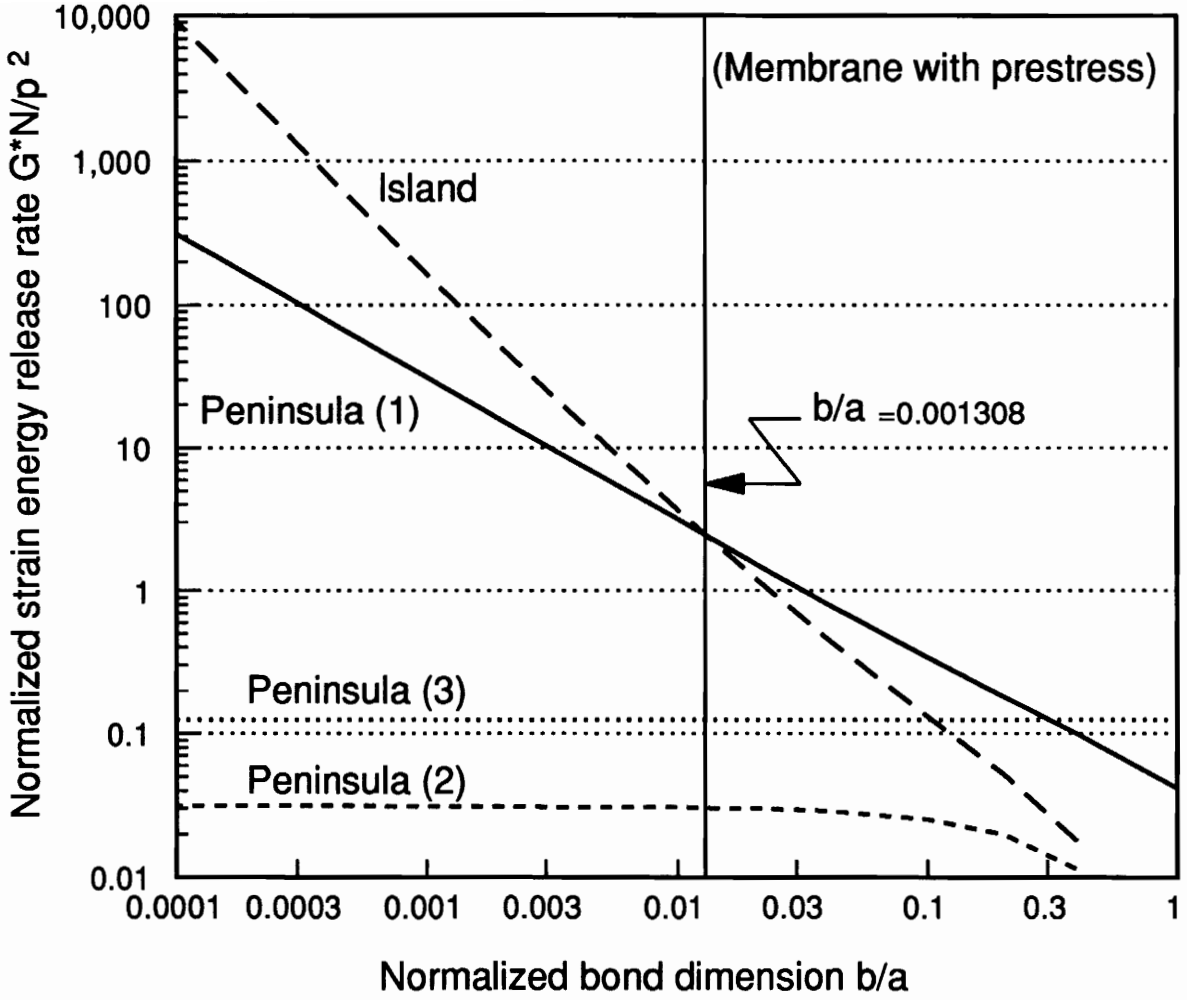

Figure 3.2.2 Effect of relative peninsula width on the strain energy release rate of the island and peninsula blister specimens

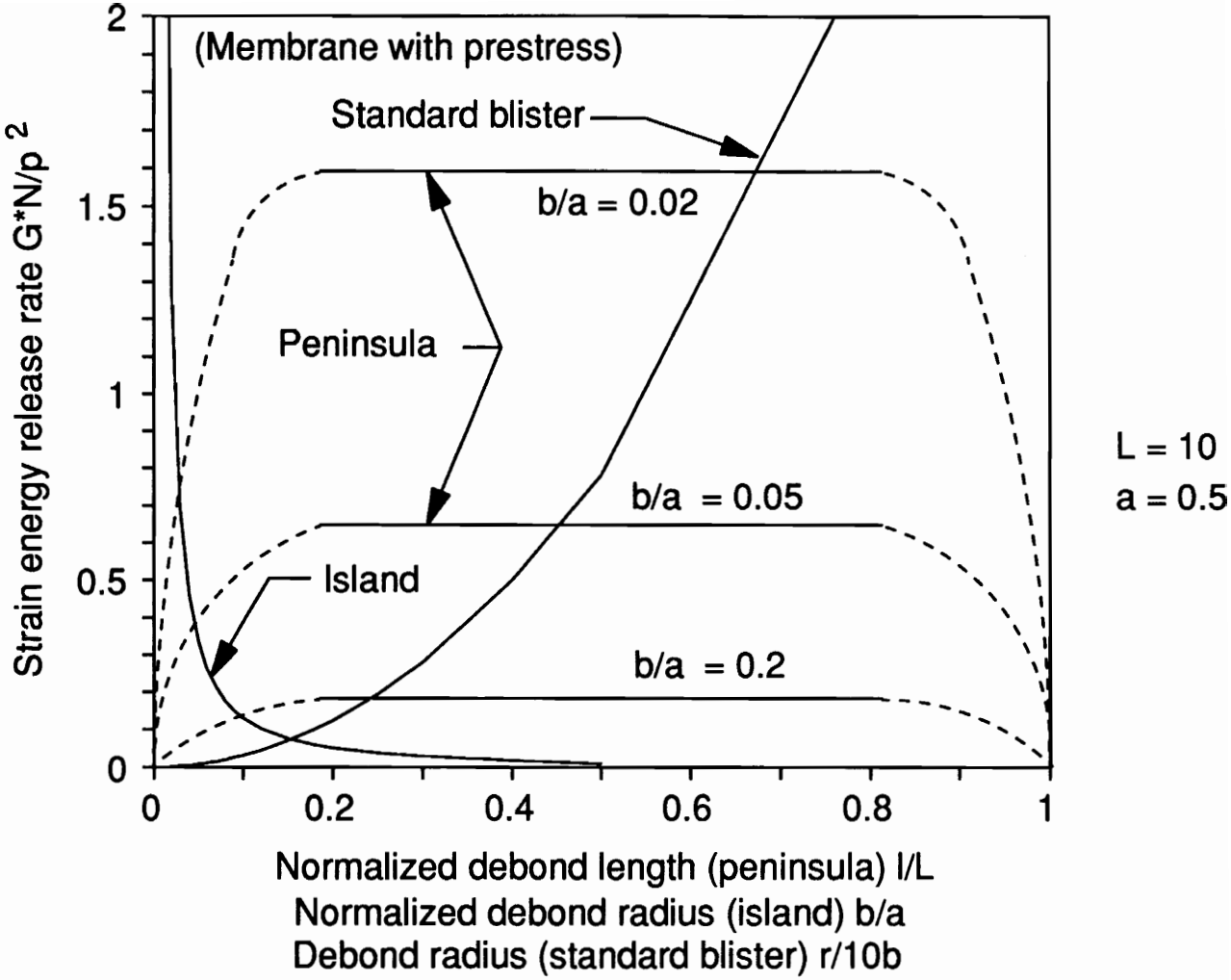

Figure 3.2.3 Variation in strain energy release rates with debond length for the standard , island and peninsula blister specimens

peninsula blister exceeds that of the island blister until the debond radius of the island blister becomes less than 0.01308 a. Below this point, the island blister outperforms the peninsula blister because of the vanishingly small debond area.

It would be interesting to contrast the island blister behavior for the plate and prestress membrane solutions. The flattening of the plate solution in Fig. 3.1.4 at very small debond radii is believed to come from the requirement that plate slopes must be continuous. Further reductions in small island radii do not permit additional specimen compliance. Membrane solutions do not require slope continuity, and hence, compliance changes are significantly larger. In actual applications, bending stiffness of thin "membranes" may not be negligible as bond radii become extremely small, so a deviation from equation. (3.2.8) may be expected. A comparison of the strain energy release rate variation with debond growth is given for the prestressed membrane case in Figure 3.2.3.

3.3 SOLUTION FOR MEMBRANE WITH NO PRESTRESS

For the case of a membrane without a dominant prestress, the problem becomes nonlinear and exact solutions are very difficult to determine. For our purposes, we will here present a solution for the case where there is no initial prestress. The only stresses in the membrane are associated with the stretching of the film during pressurization. For circular geometries, even this case does not yield simple closed form solutions, as is evidenced by the

slightly different answers obtained by Gent [13] and Allen [21] for the same geometry. These differences arise because of the differences in formulating the deflections for a circular blister. Fortunately, for the case of a non-prestressed rectangular blister of infinite aspect ratio, the solution for the deflection is unambiguous, and the results are provided below. Unlike the case of a dominant prestress, however, we find that the constitutive properties of the blister will now influence the deflections.

If we consider the case of a membrane of infinite length attached at supports a distance of w apart, and subject it to a pressure difference, we find that the membrane will deflect into a circular arc. The stress in the membrane is known from simple thin-wall pressure vessel theory to be:

$$\sigma_x = \frac{pR}{t} \qquad (3.3.1)$$

where, R is the radius of curvature of the deflected membrane.

Because the membrane is loaded in a plane-strain manner, the strain is given by

$$\varepsilon_x = \frac{\sigma_x}{E}(1-\nu^2) \qquad (3.3.2)$$

Using trigonometry one can develop a relationship between the strain (ε), the radius of curvature (R), and the subtended angle of the arc of the blister (θ) as:

$$\varepsilon=\frac{2R}{w}\cdot\theta-1 \qquad (3.3.3)$$

and

$$\theta=\sin^{-1}\left(\frac{w}{2R}\right)\approx\frac{w}{2R}+\frac{1}{6}\cdot\left(\frac{w}{2R}\right)^3 \qquad (3.3.4)$$

For our purposes, the trigonometric functions have been expanded as Taylor series, and assuming small deflections, we have retained only the lower order terms, which are the same orders of approximations as used by Gent [13]. This will limit the applicability of the following derivations. After these approximations, the following expressions can be obtained:

$$\varepsilon=\frac{1}{6}\left(\frac{w}{2R}\right)^2 \qquad (3.3.5)$$

$$R=\left[\frac{w^2Et}{24p(1-\nu^2)}\right]^{\frac{1}{3}} \qquad (3.3.6)$$

and

$$p=\frac{h^3Et}{12w^4(1-\nu^2)} \qquad (3.3.7)$$

where, h is the top height of the blister arc, and can be calculated as:

$$h=\left[\frac{12pw^4(1-\nu^2)}{Et}\right]^{\frac{1}{3}} \qquad (3.3.8)$$

By relating the geometry and constitutive relations, we are able to write that the volume per unit length of this membrane is given simply by

$$\overline{V} = \frac{w^{\frac{7}{3}}}{6}\left[\frac{3p(1-\nu^2)}{Et}\right]^{\frac{1}{3}} \quad (3.3.9)$$

When debonding occurs, the energy balance equation can be written as:

$$G\,\delta A = \delta W - \delta U - \delta Z \quad (3.3.10)$$

where, δ A is the variation of debond area

δW is the variation of external work done on the system

δU is the variation of stored elastic energy, and

δZ is the variation of the dissipated energy in regions away from the vicinity of the debonding tip

For some adhesion systems, failure occurs at stress much lower than that necessary to cause large-scale plastic yielding of the adherends. In these cases, it is assumed that no viscoelastic contribution involves and δZ term may be neglected. This will be demonstrated later in the measurements of polyimide film bonds. However, in some other systems (such as copper foil bonds, as will be shown in Chapter 5), there are viscoelastic contributions during pressurizations. In these cases, δZ will not be negligible, and the following derivations may not be employed.

Again, let's determine the strain energy release rates along sites 2 and site 3 first. Under a constant pressure, the variation of external work done on the system can be expressed as:

$$\delta W=\delta(pV)=p\cdot(\frac{\delta V}{\delta w})_p\cdot\delta w \qquad (3.3.11)$$

After substitution and integration, the stored elastic energy for this nonlinear system is found to be:

$$U=\frac{1}{4}pV \qquad (3.3.12)$$

So, under a constant pressure, the variation of the stored elastic energy can be expressed as:

$$\delta U=\frac{1}{4}p\cdot(\frac{\partial V}{\partial w})_p\cdot\delta w \qquad (3.3.13)$$

Rearranging the energy balance equation (3.3.10), we have:

$$G\cdot\delta A=\frac{3}{4}p\cdot(\frac{\partial V}{\partial w})_p\cdot\delta w \qquad (3.3.14)$$

Here, the variation of debonding area is:

$$\delta A=1\cdot\delta w \qquad (3.3.15)$$

After substituting (3.3.11) through (3.3.15) into equation(3.3.10) and solving the energy equation, we find the strain energy release rate for the peninsula blister specimen along sites 2 and 3 to be

$$G_2=\frac{7}{24}[p\cdot(a-b)]^{\frac{4}{3}}\cdot\left[\frac{3\cdot(1-\nu^2)}{Et}\right]^{\frac{1}{3}} \qquad (3.3.16)$$

$$G_3=\frac{7}{12}(pa)^{\frac{4}{3}}\cdot\left[\frac{6(1-\nu^2)}{Et}\right]^{\frac{1}{3}} \qquad (3.3.17)$$

It is noteworthy that G_3 is always larger than G_2 by a factor of at least 3.

Similarly, in order to determine the strain energy release rate at site 1, we also need to consider the volume per unit length of the bonded and debonded section. The total displaced volume of the specimen can be written as:

$$V=\frac{1}{6}\left[\frac{3p\cdot(1-\nu^2)}{Et}\right]^{\frac{1}{3}}\cdot\left[1\cdot(2a)^{\frac{7}{3}}+2(L-l)\cdot(a-b)^{\frac{7}{3}}\right] \qquad (3.3.18)$$

The variation of debonding area here is:

$$\delta A=2b\cdot\delta l \qquad (3.3.19)$$

Following a similar procedure as used in the plate and prestressed membrane case, we can obtain the strain energy release rate at site 1:

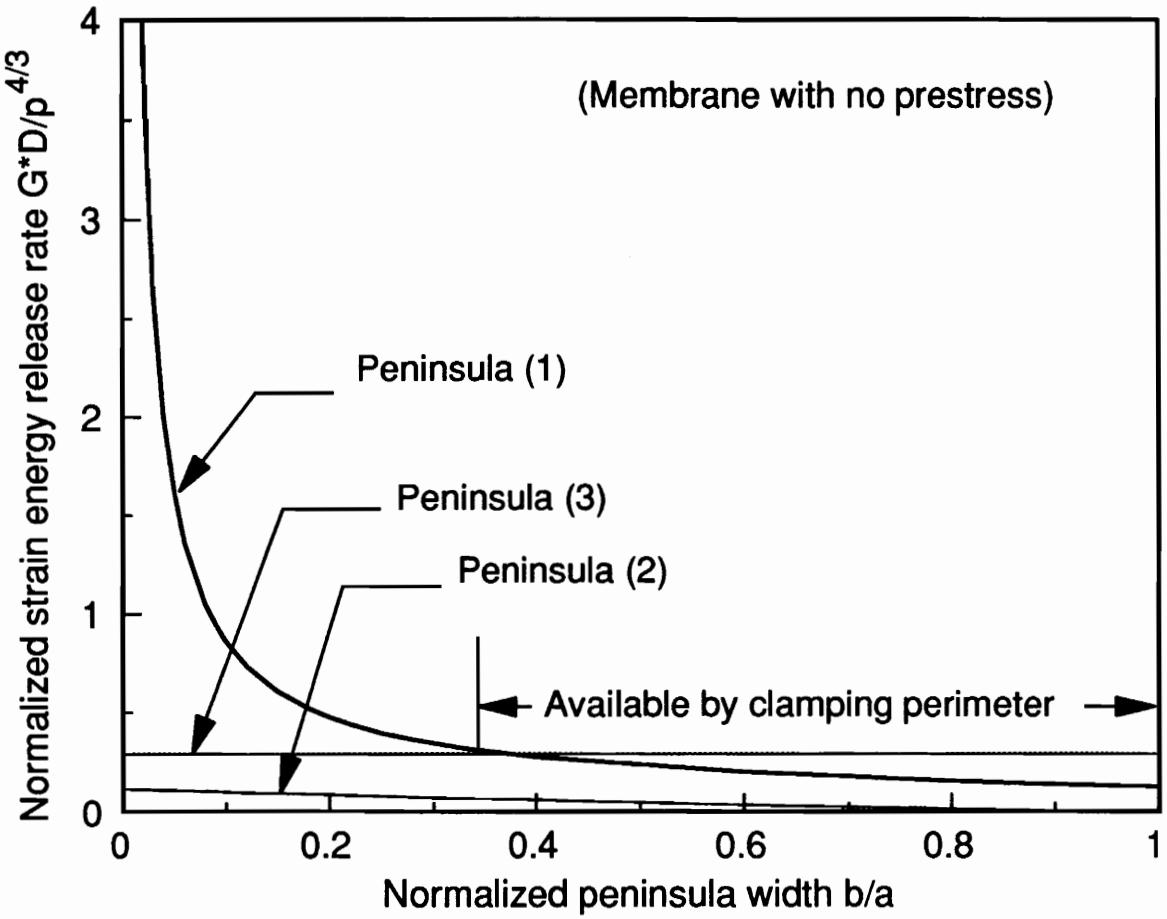

Figure 3.3.1 Effect of relative peninsula width on the strain energy release rate of the peninsula blister specimen

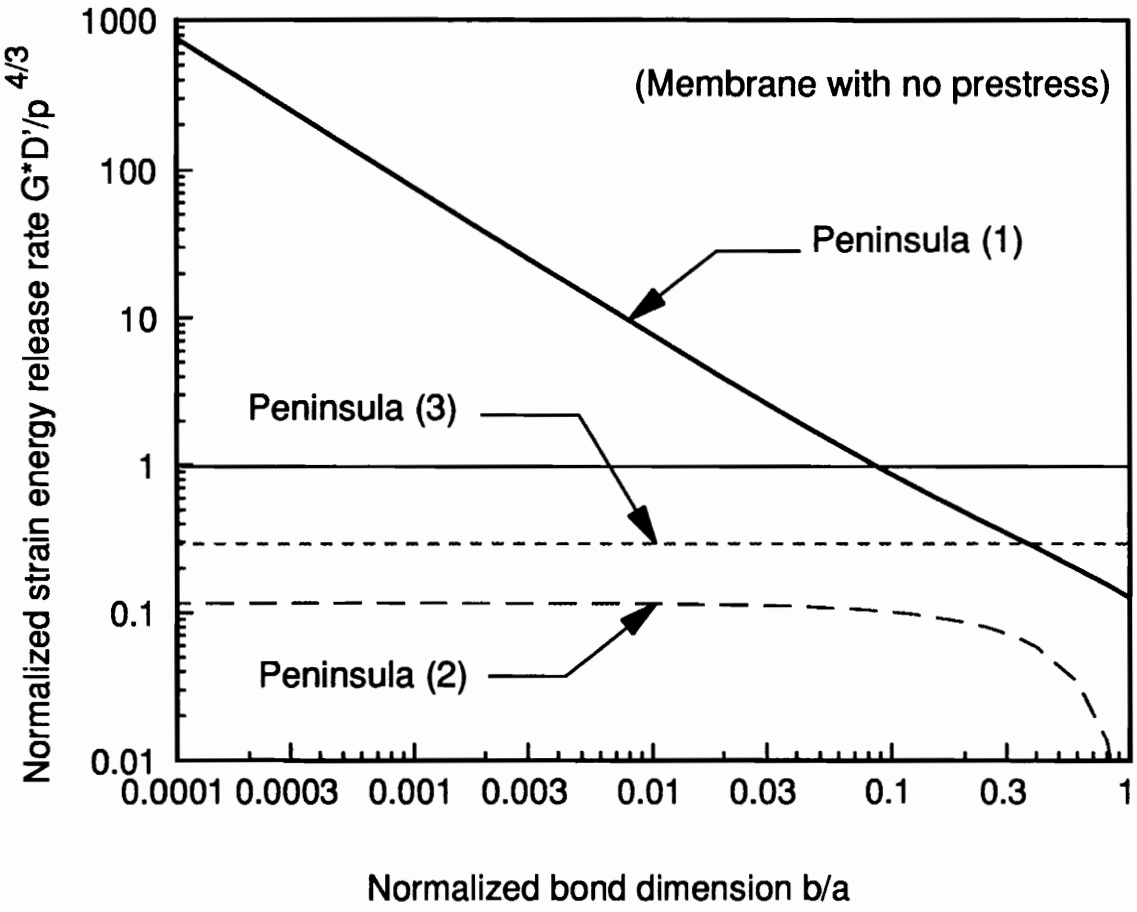

Figure 3.3.2 Effect of peninsula width on the strain energy release rate of the peninsula blister specimen

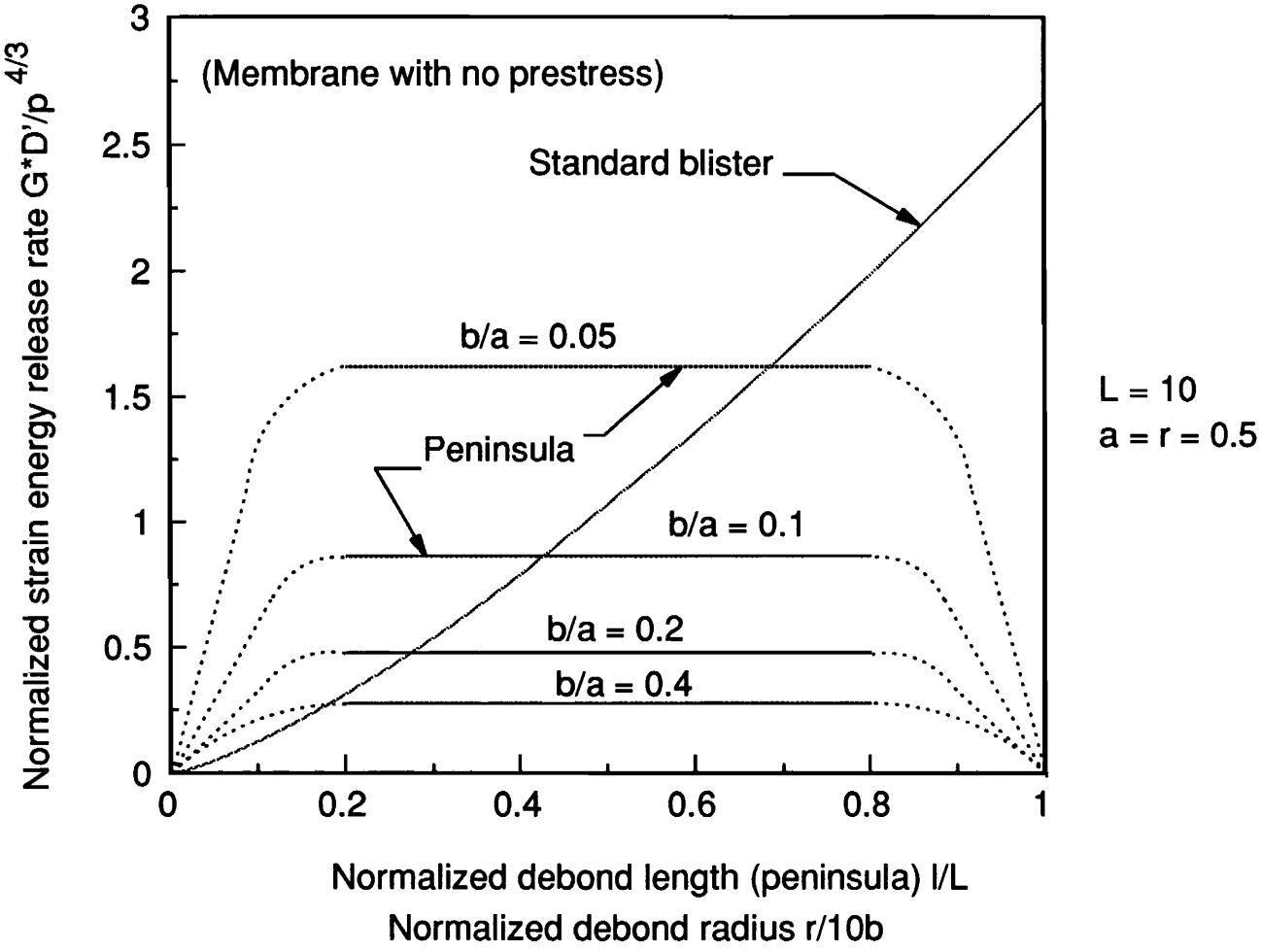

Figure 3.3.3 Variation in strain energy release rate with debond distance for the peninsula and the standard blister specimens

$$G_1=\frac{1}{16b}p^{\frac{4}{3}}\cdot\left[\frac{3(1-\nu^2)}{Et}\right]^{\frac{1}{3}}\cdot\left[(2a)^{\frac{7}{3}}-2(a-b)^{\frac{7}{3}}\right] \quad (3.3.20)$$

Again, we can see that debonding along the peninsula length always occurs instead of across the width. Also, we can find that debonding at site 1 is more likely than at site 3 for b < 0.4 a. These results are illustrated in Figure 3.3.1 and Figure 3.3.2, where the strain energy release rate has been normalized as $G^*D'/p^{4/3}$, where D' is given by

$$D'=\left[\frac{Et}{3(1-\nu^2)}\right]^{\frac{1}{3}}$$

A comparison of the strain energy release rate variation with debond growth for peninsula and standard blister for non-prestressed membrane case is shown in Figure 3.3.3. Similar conclusions can be drawn here as in the previous cases of plate and membrane with dominant prestress.

Due to several approximations employed in this no prestress membrane derivations, the above solutions are valid under limiting cases. These limitations include:

(1) The blister deflections are small. If the deflections are not small enough, the neglection of the lower order terms of the Taylor's series expansion in equation (3.3.4) may lead to errors. In this case, the

membrane strains calculated by the above method will be smaller than the true values of the membrane strains, and the predicted variation of blister volume changes during debonding will be smaller. Therefore, the predicted strain energy release rates from the above derivations will be smaller than the true values of the strain energy release rates.

(2) No prestress exists in the film. If a dominant prestress exists in the film, solutions obtained in section 3.3 are recommended. If a very small amount of residual stress exists in the film due to specimen fabrication, and the residual stress is so small that it can be neglected, the solutions in this section are still valid approximations.

(3) Before application of pressure, the original shape of the film is flat. Section 3.4 will discuss the case when there is initial slack in membrane.

3.4 SOLUTION FOR MEMBRANE WITH INITIAL SLACK

The non-prestressed membrane discussed in section 3.3 is an ideal case. In actual application, it is not always easy to fabricate a perfectly flat and non-stressed film adhering onto the substrate. The reasons are many. For example, if the adhesive or film needs to be cured under high temperatures, differences of the thermal expansion coefficients between the substrate and the membrane may cause either residual stress or initial slack in the membrane. In the case where no high temperature is involved, manual fabrication of a thin film onto a substrate still could cause initial slack or residual stress in varying degrees. Exact solutions for these two cases, i.e. initial slack or

residual stress, are very difficult to obtain. For our purposes, we here consider limiting cases. The limiting case for a membrane with residual stress is the case where the prestress is dominant, and the applied pressures and blister deflections are so small that the additional membrane stresses induced by stretching can be neglected when compared to the initial residual stress. This case has been discussed in section 3.3. The limiting case for a membrane with initial slack is that when pressurized, the initial slack dominates and the stretching of the film can be neglected. For simplification, herein, we only derive the strain energy release rate along the peninsula length (site 1).

Similar to the previous sections, we assume infinite length. If the width of each blister region in the membrane is w, as shown in Figure 3.4.1(a), the total membrane width in the blister region equals 2w + 2b, which remains the same after debonding, as assumed.

The volume per unit length of each blister before debonding, as shown in Figure 3.4.1(a), can be expressed in terms of w and a as:

$$\overline{V} = \frac{Rw}{2} - a\sqrt{R^2 - a^2}$$

$$= \frac{\frac{1}{2}w^{\frac{5}{2}} - a\sqrt{w^2 - 24a^2w + 48a^3}}{2\sqrt{6(w-2a)}} \qquad (3.4.1)$$

So, the volume per unit length before debonding is:

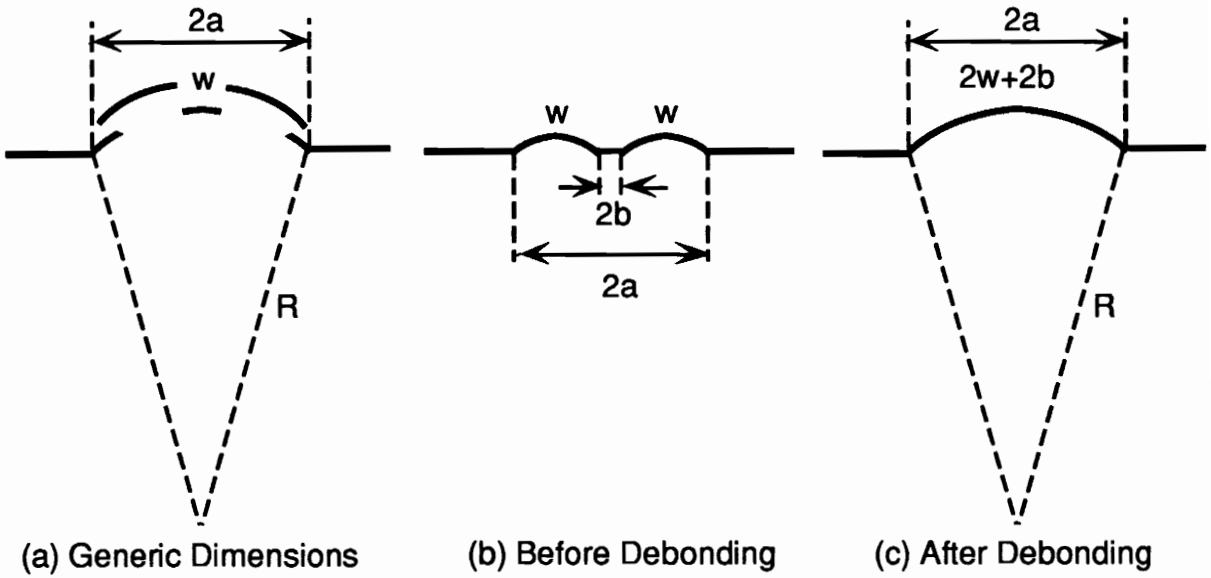

Fig. 3.4.1 Diagram of a Membrane With Initial slack

$$\overline{V}_{bonded} = \frac{\frac{1}{2}w^{\frac{5}{2}} - \frac{(a-b)}{2}\sqrt{w^3 - 6(a-b)^2 w + 6(a-b)^3}}{\sqrt{6(w-a+b)}} \qquad (3.4.2)$$

The volume per unit length after debonding is:

$$\overline{V}_{debonded} = \frac{(w+b)^{\frac{5}{2}} - a\sqrt{(w+b)^3 - 6a^2(w+b) + 6a^3}}{\sqrt{6(w-a+b)}} \qquad (3.4.3)$$

Therefore, the volume change after debonding can be obtained:

$$\delta V = (\overline{V}_{debonded} - \overline{V}_{bonded}) \cdot \delta l$$

$$= \frac{(w+b)^{\frac{5}{2}} - a\sqrt{(w+b)^3 - 6a^2(w+b) + 6a^3} - \frac{1}{2}w^{\frac{5}{2}} + \frac{(a-b)}{2}\sqrt{w^3 - 6(a-b)^2 w + 6(a-b)^3}}{\sqrt{6(w-a+b)}} \cdot \delta l$$

(3.4.4)

Applying the energy balance equation (3.3.10), and substituting terms of the variations of strain energy and debonding area (for this case, $\delta U = 0$ and $\delta A = 2b\,\delta l$), the strain energy release rate along the peninsula length can be determined as:

$$G_1 = \frac{\delta W}{\delta A} = \frac{p}{2b} \cdot \frac{\delta V}{\delta l}$$

$$= \frac{p}{2b} \cdot \frac{(w+b)^{\frac{5}{2}} + a\sqrt{(w+b)^3 - 6a^2(w+b) + 6a^3} - \frac{1}{2}w^{\frac{5}{2}} + \frac{(a-b)}{2}\sqrt{w^3 - 6(a-b)^2 w + 6(a-b)^3}}{\sqrt{6(w-a+b)}}$$

(3.4.6)

It is interesting to note that there is no material constitutive properties involved here, again.

Figure 3.4 depicts the effects of initial length to the strain energy release rate for peninsula blister specimens. It can be seen, from Figure 3.4, that under a constant pressure, the larger the initial slack length, the higher the strain energy release rate produced by the peninsula blister specimen.

This solution, as well as the others discussed in the previous sections 3.2 and 3.3, are limiting cases. Usually, an actual case for membrane-like films is either between cases 3.2 and 3.3 if there are residual stresses involved, or between 3.3 and 3.4 if initial slack exists after specimen fabrication. If the residual stress in the film is very large compared to the stress due to pressurization, as in Allen and Senturia's island blister test, solutions in section 3.2 may be used. If there is no or very low initial prestress involved during specimen fabrications, solutions in section 3.3 may be applied to predict the strain energy release rates. The experimental studies performed in this research fall in the category of membrane with no prestress discussed in section 3.3.

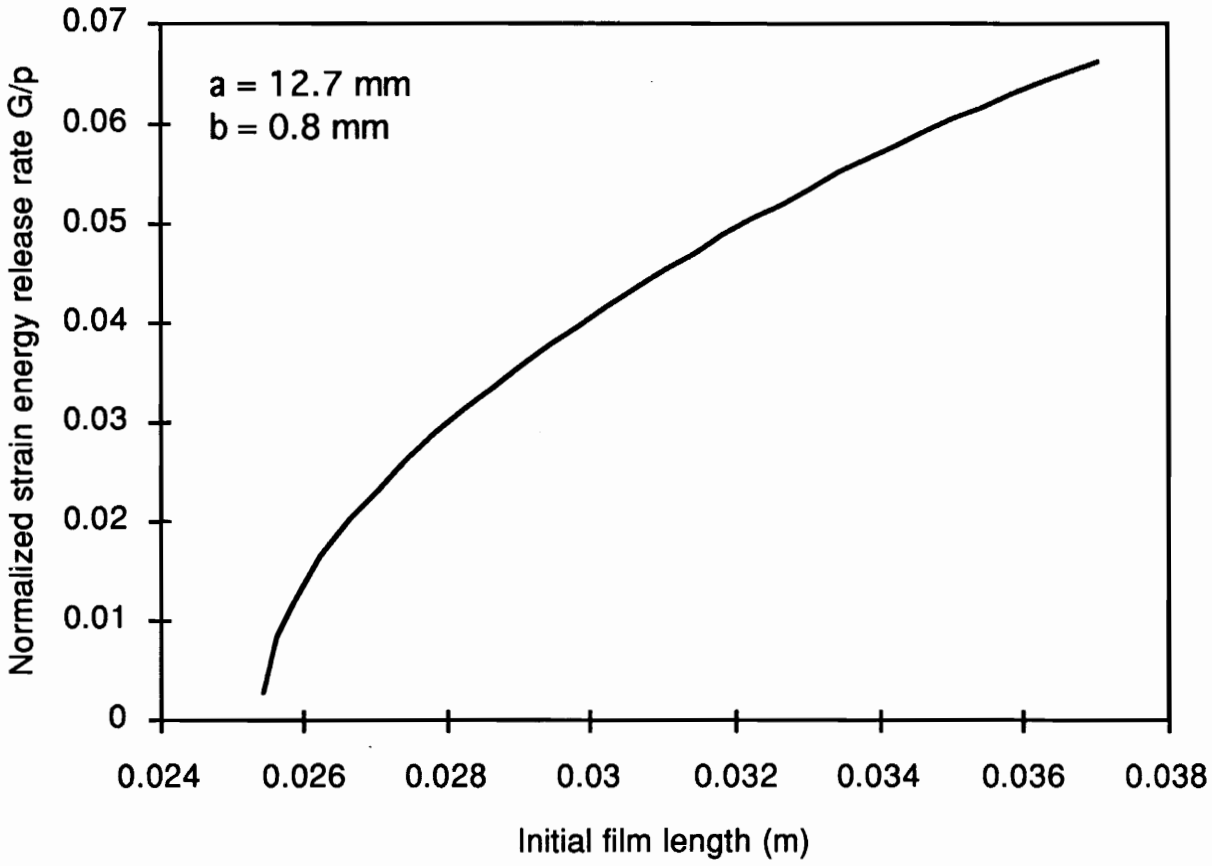

Figure 3.4 Effect of initial slack on the strain energy release rate of the peninsula blister specimens

3.5 STRESS ANALYSIS

From the above analysis, one may conclude that, at a given pressure, the peninsula blister specimen not only produces a constant strain energy release rate along the major portion of the peninsula, but also obtains high strain energy release rates by making the normalized peninsula width (b/a) smaller. The advantages of constant strain energy release rate have been discussed in the introduction chapter. Questions may be raised on whether it is possible to obtain a higher ratio of strain energy release rate to membrane stress for this modified blister specimen. When testing adhesion of well-adhered thin film bonds with low tensile strength, films often burst before debonding can initiate. By applying the peninsula blister specimen and making b/a small enough, debonding can take place at relatively low pressures. Will the membrane stress be reduced by this geometrical modification? This question is significant when testing the adhesion of thin film bonds because if the answer is positive, film ruptures could be reduced by altering specimen geometries. In order to answer this question, it is necessary to develop relations between strain energy release rate and membrane stress of the testing specimens.

Unlike the axisymmetric geometries in circular blister specimens (standard, island, and constrained) , the peninsula blister geometry is very difficult to model, thus, closed form solutions or numerical solutions for stress distributions along the blister film (membrane case) are not easy to obtain. As stated in the previous chapters, island blister specimens also have the characteristic of high ratio of strain energy release rate to applied pressure.

As an extension of the island blister specimen, the debonding behavior for a peninsula blister specimen at the debonding front is very similar to that for an island blister specimen. If island blister has the ability of geometrically overcoming the tensile strength limitation, the peninsula blister specimen should behave similarly.

Let us first consider a standard blister specimen for the case of a membrane with no prestress, as shown in Figure 1.3. By using Gent's solution [13], the strain energy release rate can be expressed as:

$$G=\frac{5}{8}\left[\frac{3(1-\nu)}{8Et}\right]^{\frac{1}{3}}\cdot(pa)^{\frac{4}{3}} \qquad (3.5.1)$$

where, a is the blister radius, and E, t and ν represent Young's Modulus, thickness and Poisson's ratio of the film, respectively. From this equation, one might infer that a high ratio of strain energy release rate to applied pressure can also be obtained by making the blister radius larger. However, if we relate the strain energy release rate (G) and the membrane stress (σ) in the pressurized blister film, the following expressions can be obtained:

$$G=\frac{15\cdot\sigma^2(1-\nu)t}{2E} \qquad (3.5.2)$$

It can be seen, from equation (3.5.2), that the ratio (G/σ^2) is independent of specimen geometry, blister radius (a). In other words, by making the blister radius (a) larger, the ratio of strain energy release rate to applied pressure could be raised, but the membrane stress will also increase accordingly.

Therefore, for a standard blister specimen, it is impossible to obtain high G without increasing membrane stress by simply modifying specimen geometry.

Similar studies have also been conducted to analyze the peel test specimen. The relation between strain energy release rate and membrane stress for a thin film peel specimen with fixed take-off angle θ, as shown in Figure 1.2, can be expressed as:

$$\sigma_s = E\cdot\left[\sqrt{(1-\cos\theta)+\frac{2G}{Et}}-(1-\cos\theta)\right] \qquad (3.5.3)$$

For a standard peel ($\theta = 90^o$) specimen, this equation becomes

$$\sigma = \frac{G}{t} \qquad (3.5.4)$$

No geometry factor (specimen width w) is involved in these two equations, implying that one is not be able to raise G without increasing the membrane stress by changing geometry factors. This agrees well with the result obtained from the standard blister specimen.

The above analysis for the standard blister geometry and peel test specimen suggests that, when testing adhesion of thin film bonds with these geometries, film ruptures can't be reduced by altering geometries. In fact, if we only consider the very localized debond region, one may conclude that, for same adhesively bonded joints with same peel angle, free body diagrams at the localized debond regions for all kinds of blister specimens and peel specimens

are very similar, as shown in Figure 3.5.1. Therefore, the debonding behaviors should be similar, and the strain energy release rate should be determined only by the membrane stress and peel angle. In other words, in order to reach the critical strain energy release rate, the required membrane stresses should be the same, and any far field geometry aspects shouldn't be able to change the ratio of strain energy release rate to membrane stress.

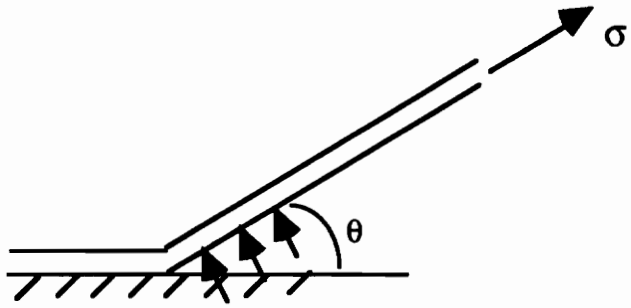

Figure 3.5.1 Free Body Diagram for Blister Specimen and Peel Specimen at Local Debond Region

However, during the development of the island blister specimen, Mark Allen [28] claimed that the ratio of strain energy release rate to membrane stress (strain) can be increased by altering the specimen size for his blister test technique. He analyzed the island blister specimen for the case of thin membrane with dominant prestress, and calculated the strain energy release rate and the average value of membrane strain in the pressurized annular film. According to his derivation, the relation between the ultimate strain

(ε_{ult}) of the film and the maximum strain energy release rate that can be measured from the island blister specimen (G_{max}) could be expressed as:

$$G_{max}=\sigma_o \cdot t \cdot \varepsilon_{ult} \cdot \left(\frac{(\phi-2)^2}{\frac{\phi^2}{\beta}-4\phi+\frac{4}{3}\frac{\beta^3-1}{\beta-1}} \right) \qquad (3.5.5)$$

where, t is the film thickness, 2b is the island radius , 2a is the outer radius, σ_o represents the residual stress in the film, the geometry factor β is defined as β = a/b, and ϕ is defined as $\phi=\frac{(\beta^2-1)}{\ln\beta}$.

It was found, from the plot of the normalized strain energy release rate ($\frac{G_{max}}{\sigma_o t \cdot \varepsilon_{ult}}$) versus geometry factor (β), that the relation of ($\frac{G_{max}}{\sigma_o t \cdot \varepsilon_{ult}}$) and β was almost linear. Therefore, he concluded that, for thin film bonds with arbitrarily strong adhesion, debonding can be initiated without rupturing the film by making the geometry factor (β = a/b) large enough.

Experimental results for the adhesion measurement of polyimide films spin-coated on microelectronic structures had been carried out by Allen, and the results supported his conclusion. It was found that films often burst before debonding initiated if the samples were fabricated on standard blister sites. However, when the samples were fabricated on island blister sites with a large β ratio, he succeeded in measuring the debonding without film rupture. From his analytical and experimental results, the island blister test seems to be

much better than the standard blister and the peel test for testing adhesion of thin film bonds.

Another example is the constrained blister geometry, which has been introduced in Chapter 1. Moet, et al. [19] claimed that the constrained blister geometry also had the ability of overcoming the film rupture by altering the height of the constraint. According to his analysis, the stretching of film can be reduced by the constraint placed on top of the blister. This constraint limits the large vertical deflections of the blister and requires that larger pressures be applied. However, the analytical analysis of the relations between strain energy release rate and membrane stress along with geometry variables for the constrained blister geometry are not available in the literatures.

The claims made by Allen and Moet contradict the conclusions one may draw based on a free body diagram of the local debond region. Is it possible to overcome the tensile-strength limitations by modifying specimen geometries? If the answer is negative, how does one explain the experimental success of Allen's island blister test? If positive, how does one explain the free body diagram of the local debond region shown in Figure 3.5.1.

An attempt has been made to examine Allen's calculation for island blister geometry. Primarily, his solutions were based on the assumption of a dominant prestress and low applied pressure. It was assumed that the film behavior was dominated by its inherent residual stress, and the in-plane membrane stress induced by pressurization was neglected. Therefore, the stress distribution all over the blister film was assumed to be uniform and

equal to the residual stress during pressurizing. By making (a/b) large enough, the critical strain energy release rate could be reached at a very low pressure. In this case, if the membrane stress induced by this pressure was still much less than the prestress, debonding could be initiated without rupturing the film. However, his conclusions may be questionable if membrane stress is not dominated by the prestress.

For the case where prestress does not dominate, the in-plane membrane stress induced by pressurization can't be neglected. The membrane equilibrium equation becomes nonlinear, and closed form solutions are very difficult to obtain. In order to solve these problems, numerical methods were applied. According to the recent finite element analysis by Lai [29], a typical membrane stress distribution along a pressurized island blister film is as shown in Figure 3.5.2. This is an example of a membrane with prestress σ_o (30 MPa), applied pressure p (=6.0 KPa) and geometry factor β (= 10). It can be seen clearly that stress concentration exists around the debonding front of the island despite the fact that the membrane is dominated by prestress at regions far away from the island. Similar stress distributions were seen for the case of membrane without prestress. Figure 3.5.3 depicts relations of the normalized stress ($\sigma_{max}/\sigma_{ave}$, or $\sigma_{max}/\sigma_{res}$) versus geometry factor β for cases of membranes with and without prestress. It should be noted that in the case of membrane without prestress, the applied pressure used in this analysis was 6 Pa. Here, σ_{max} (S_m), σ_{ave} (S_a) and σ_{res} (S_r) are defined as the maximum stress, average stress and residual stress, respectively. These results suggest that normalized stresses also increase with the increase of geometry factor, especially for lower prestress cases. In order to approximate the relations

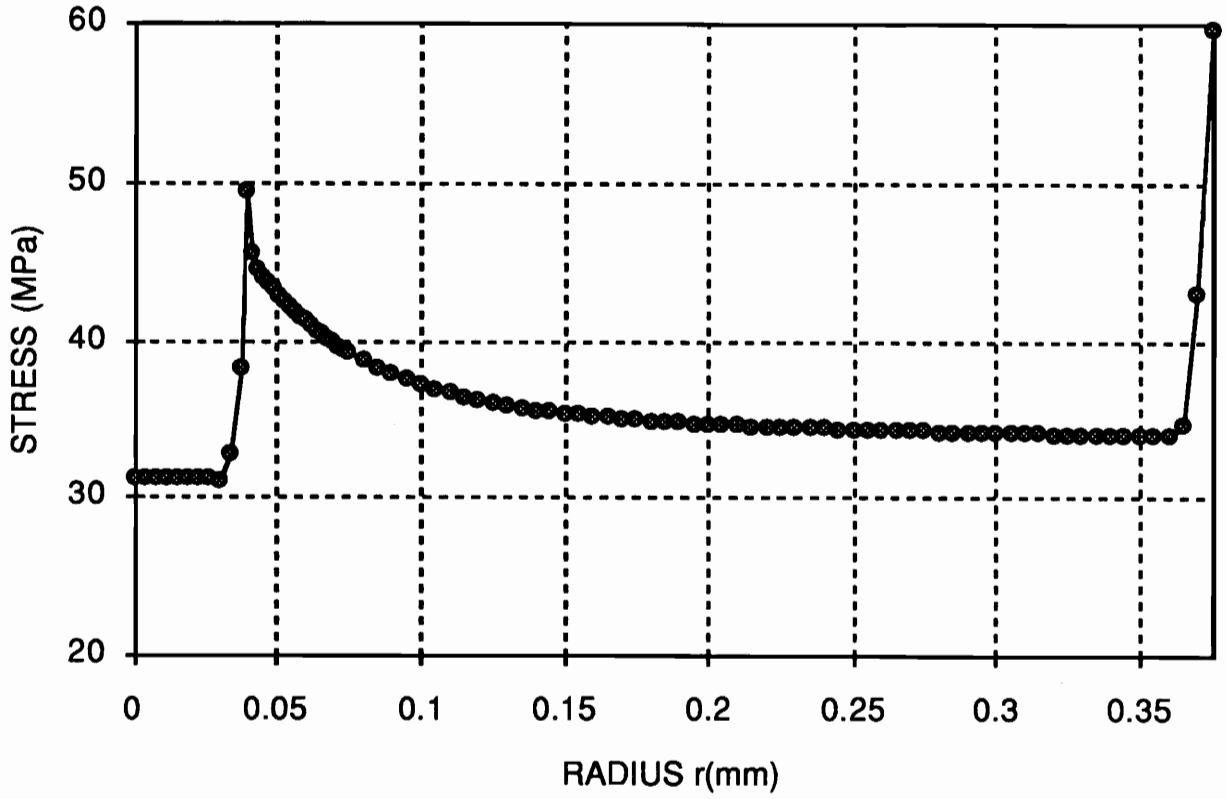

Figure 3.5.2 Membrane Stress Distribution for Thin Film Island Bliser Specimen with Prestress (a/b=10, b=37.5mm, p=6KPa, t=0.5mm, Sres=32MPa)

between the membrane stress and the geometry factor, curve fitting was conducted and the result was found to be in the form of:

$$\frac{\sigma_{max}}{\sigma_{ave}} = C \cdot \beta^{\lambda} \qquad (3.5.6)$$

where, C and λ are functions of material properties, residual stress and applied pressure. From the fitting results, λ equals to 0.38 and 0.32 for the cases of p = 6000 Pa., σ_0=30 MPa, and p = 6 Pa, σ_0 = 0, respectively. This implies that the maximum membrane stresses increases more rapidly with the geometry factor if the prestress is lower. If the relations between the strain energy release rate and geometry factor can be found, the relations between strain energy release rate and maximum stress can be determined.

Due to the difficulties in modeling and the time limitations, relations between the strain energy release rate and the membrane stress haven't been carried out in this research. Therefore, accurate analytical solutions for island blisters are still unknown. In summary, when testing thin film bonds, if the residual stress dominates through the pressurizing blister procedure, Allen's solution is a good approximation. However, for cases of well-adhered thin film bonds with weak tensile strength and low residual stress, Allen's conclusion may not be valid. Instead of a uniform stress distribution all over the pressurized film, stress concentrations will be present at the debonding front. In addition, the stress concentration will increase when β becomes larger, therefore, the film may rupture before debonding initiates. For these cases, the above analysis suggests that island blister specimen, as well as the

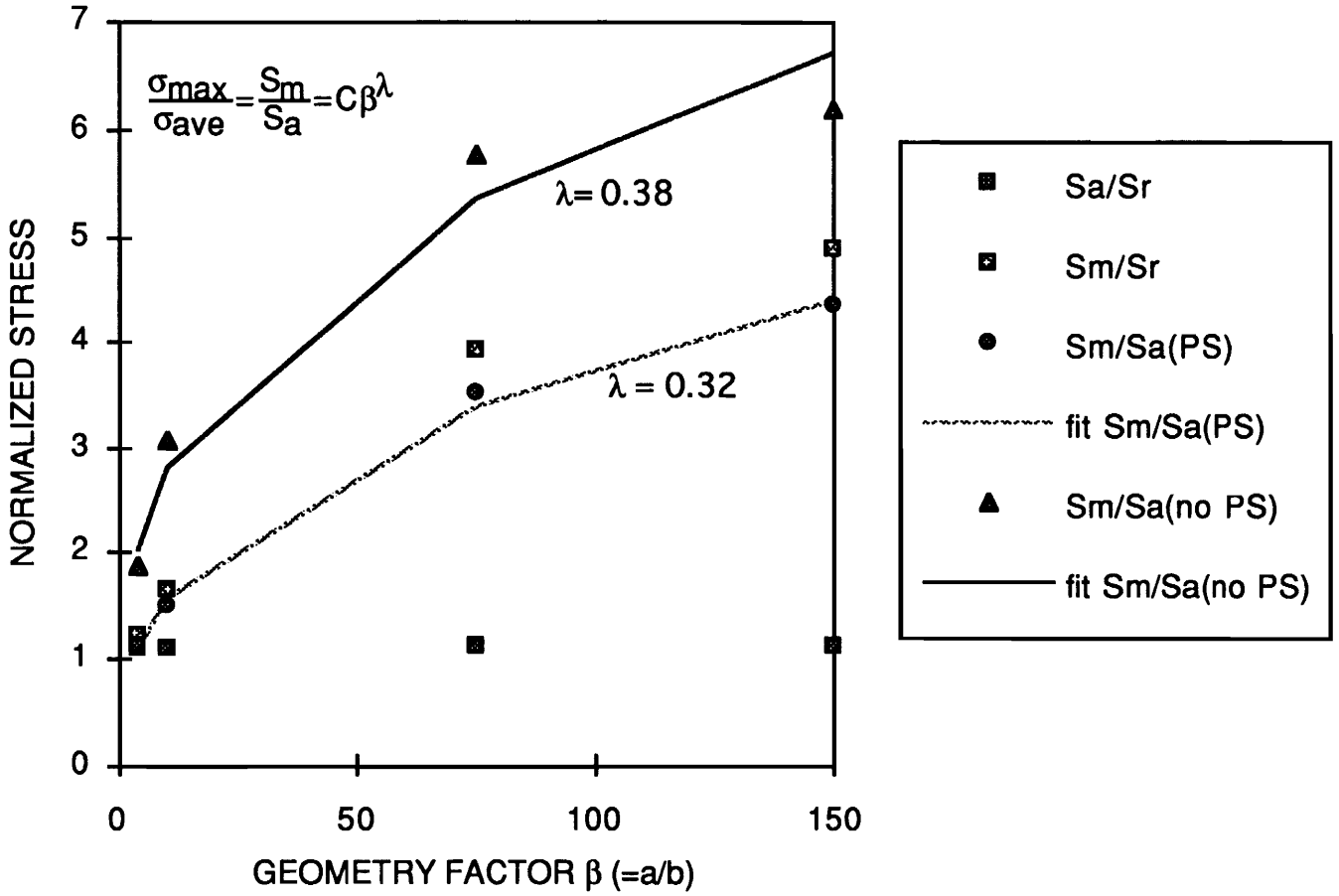

Figure 3.5.3 Normalized Stress versus Geometry Factor for a Thin Film Island Blister (Finite Element Results)

standard blister and peel test specimen, may not be able overcome the tensile strength limitation geometrically.

At the present time, no solid conclusions can be made here to answer the questions proposed previously in this section. Further investigations need to be conducted to develop accurate relations between the strain energy release rate, membrane stress and geometry factors for an island blister specimen, and furthermore, for a peninsula blister specimen.

CHAPTER 4. EXPERIMENTAL APPARATUS AND PROCEDURE

4.1. Experimental Apparatus

The primary data acquired from a mechanical or fracture test are generalized load and generalized displacement. For a blister test, these two measurements are applied pressure and blister volume. Figure 4.1 shows the specimen fixture developed for a peninsula blister test. The testing materials (thin films) were bonded onto the peninsula and the outer perimeter of the substrate, thus forming an enclosed groove. In order to apply pressure, the groove in the substrate was connected to the pressure system. In order to measure the blister volume, a spacer and a transparent plate were mounted on the top of the specimen, thus forming another enclosed cavity. Rubber gaskets were used to seal the cavity. The plate was made of polycarbonate to permit visual observation. The spacer was also employed as a clamp in order to prevent debonding along site 3, as mentioned in Chapter 3. The cavity, which was filled with water, was connected to a calibrated glass tube so that the volume of a growing blister could be measured by recording the displaced water volume rising in the glass tube.

Figure 4.2 is a schematic diagram of the experimental apparatus. This testing system is composed of a pressure source, a pressure transducer, a fine nupro needle valve, a release valve, some necessary tubing, a calibrated glass tube, a video camera, a cassette recorder with a timer, and the data acquisition system.

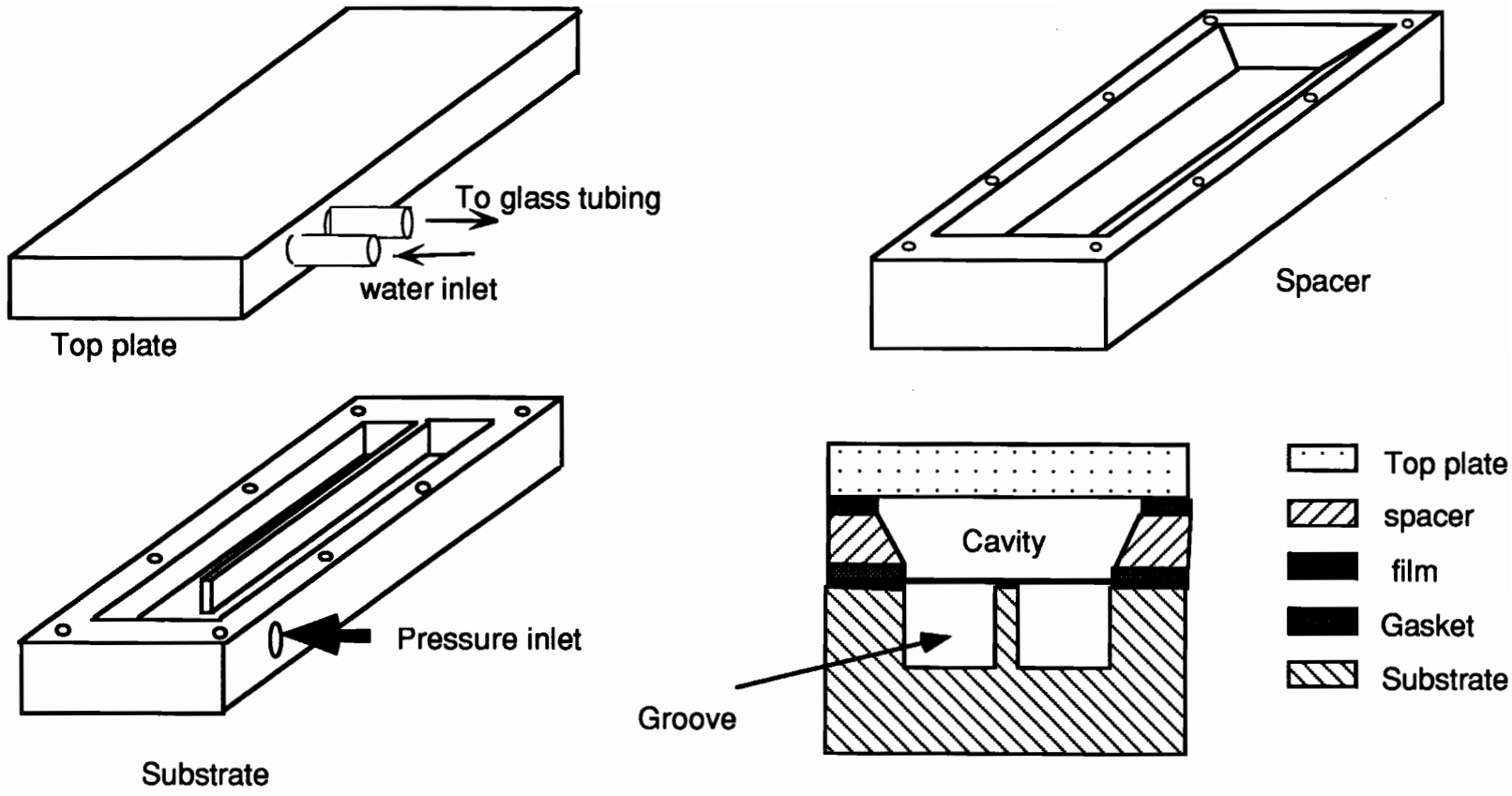

Figure 4.1 Testing Fixture for Peninsula Blister Test

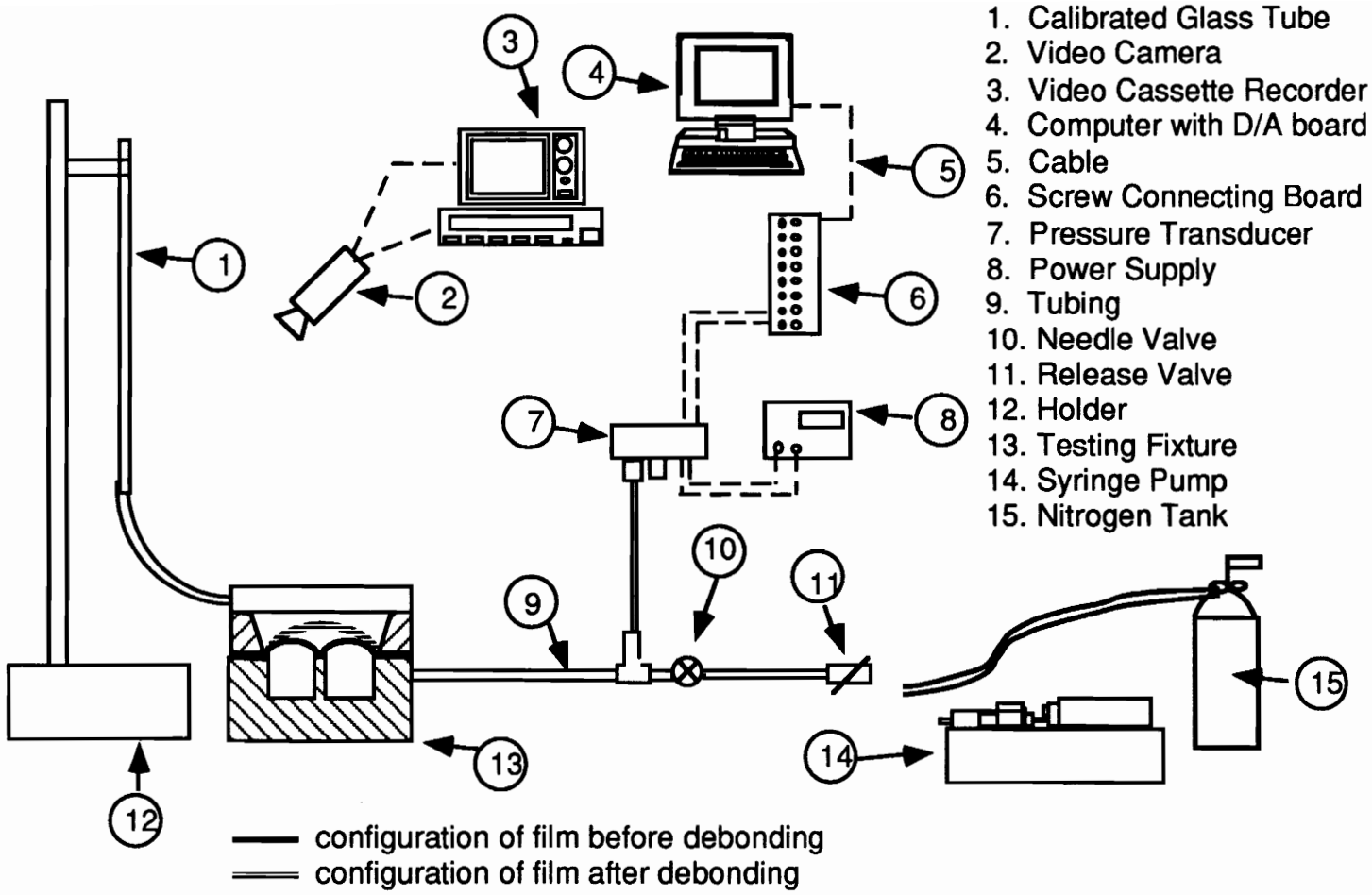

Figure 4.2 Schematic Diagram of Experimental Setup

The pressure source could be either a nitrogen tank for pneumatic pressure, or a syringe pump for hydraulic pressure. Although the syringe pump was supposed to result in a constant flow rate control during loading, preliminary experiments showed that a little bit of leaking or air bubbles in the substrate groove or connecting tubings might cause large inaccuracy of the blister volume measurements. Thus, a nitrogen tank was chosen in the current study. In addition, pneumatic pressure (nitrogen tank) was selected instead of a syringe pump to avoid the effects of water penetration into the peninsula testing interface.

Real time pressure data was recorded continuously by an IBM compatible personal computer. In order to convert the electrical signals into digital signals, an analog/digital (A/D) board, Model DT 2805 manufactured by Data Translation, Inc., was employed to interface between the output of the pressure transducer and the input of the computer. A computer program written in Quick Basic coordinated the data-acquisition process. Recorded data was then imported into a spreadsheet file for analysis.

Blister volume data was obtained through a calibrated glass tube. Preliminary tests suggested the selection of a calibrated glass tube 7 mm diameter and 70 mm in length for the testing materials and the geometry utilized in this study. The debonding process and the blister volume data were monitored with a video camera and was recorded as a function of testing time with a video tape recorder.

The pressure transducer, Omega Corporation Model 142PC30D, used in this research had a nominal range of 0-30 psi. This transducer was calibrated using a standard mercury manometer setup with the reference side of the manometer open to the atmosphere at room temperature. The manometer used here was borrowed from the Electronics Shop of the Mechanical Engineering Department on campus. During calibration, the power supply was set at +10V excitation and the transducer gave 1-6V output range. While taking data, the excitation voltage was set to the same value as during calibration. The pressure to voltage calibration yielded a sensitivity of 4.74 psi/volt (32.67 KPa/volt).

4.2. Testing Procedure

The samples were mounted in the specimen fixture as depicted in Section 4.1. After pressure was introduced into the groove through the needle valve; the thin film flexed as indicated in Figure 2.1(b). The needle valve was set to maintain a low flow rate during testing. The applied pressure was raised by slowly adjusting the regulator on the nitrogen tank. When the pressure reached the critical value, debonding would proceed along the peninsula length after initiating at the tip of the peninsula. It will be shown later that the debonding behavior was different for elastic materials and viscoelastic materials. Figure 2.1(c) illustrates the deflection of the film after debonding. After debonding along the peninsula was completed, the pressure was reduced by setting the release valve free. The needle valve was set at the same flow rate as used during loading procedure. During these loading, debonding and

unloading procedures, pressure and volume data as functions of testing time were recorded. Presumed pressure versus volume curves and interpretation of these data to the adhesion measurement and mechanical property measurement will be shown in the next section. Typical results for the measurement of some thin film bonding systems will be presented and discussed in Chapter 5.

4.3 Data Analysis Method

(a) Pressure-Volume Behavior

Figure 4.3 shows a typical pressure-volume data expected for a peninsula blister specimen. This characteristic curve is divided into three regions; the loading region, the debonding region and the unloading region. Brief descriptions of each region will be given below.

In the loading region, line 1, no debonding has occurred. At point A, pressure is applied and the blister starts expanding. As the applied pressure increases, the blister volume follows along line 1 until the critical pressure is reached at point B, which is the onset of debonding. During this loading region, the shape of the test specimen is unchanged but the magnitude of the blister volume is increased.

At the debonding onset point, B, debonding along site 1 at the film-substrate interface starts and the debonding region is entered. In this region, debonding behavior of different testing materials should be varied. If the

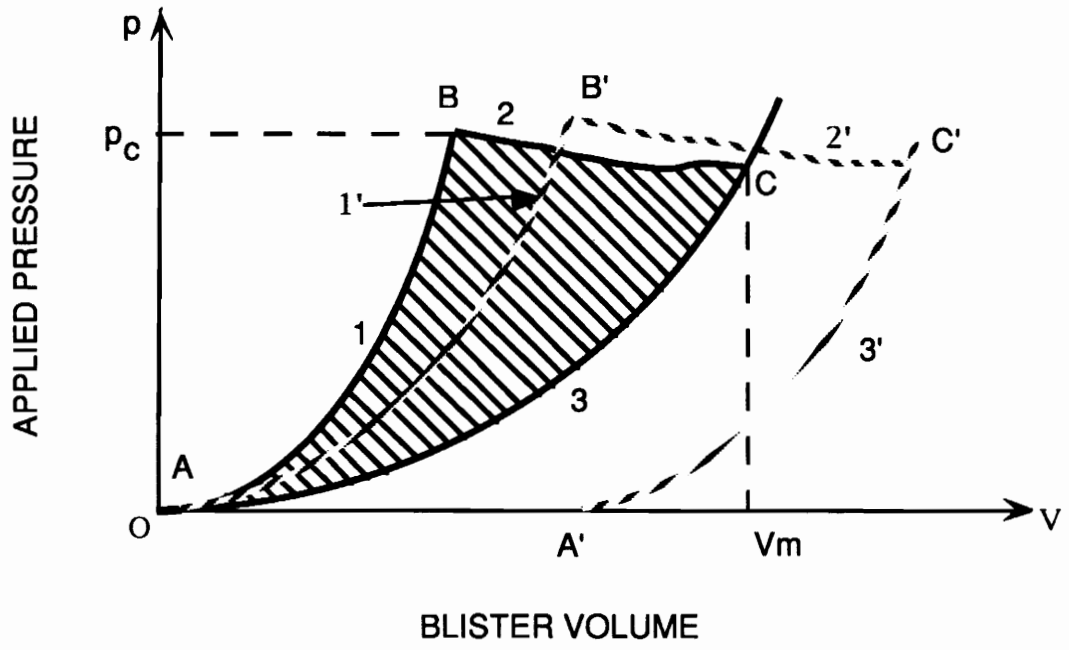

Figure 4.3 Typical Pressure-Volume Behavior for a Peninsula Blister Test

adhesives are viscoelastic materials, for instance, pressure sensitive adhesives (PSA), stick-slip phenomenon will be observed. And the mechanical and fracture behaviors of these materials will depend on many factors, such as temperature, time and loading rate. If the adhesive and the blister films are very brittle, their behaviors will be elastic instead of viscoelastic. The dependence of time, temperature or loading rate would not be significant, and the debonding will proceed more rapidly. But, for all adhesives and films, the debonding rate should be independent of debond length along the major portion of the peninsula length due to the constant strain energy release rate nature of this peninsula blister specimen.

At point C, debonding along the peninsula length is fully completed. If no plastic deformations occurs during the loading procedure, releasing the pressure should result in a pressure - volume relation which follows line 3 until point A is reached again, and the testing cycle is completed. This is the unloading region.

If the film adherend is plastically or viscoelastically stretched during the loading procedure, the pressure - volume behavior will be different. As shown in Figure 4.3 in dotted curves, starting from the original point, A, the loading curve will shift right by following line 1' instead of line 1. The critical pressure will not be the same as the non-plastically-stretched case. The unloading line will also shift right by following the dotted line, 3', and ending at point A'. The larger the plastic deformation is, the larger the shift level will be.

(b) Methods to determine the strain energy release rates

There are two ways to determine the strain energy release rate with the pressure and volume data obtained from a peninsula blister test: analytical method and experimental compliance method. A brief description of each method will be given below.

Analytical method

From our theoretical solutions, the strain energy release rate for the case of a membrane without prestress and initial slack is given by equation(3.3.5). Therefore, analytical values of G can be obtained by measuring the specimen dimensions a and b, Young's modulus E, Poisson's ratio ν, the film thickness t, and the critical debonding pressure p_C. The critical pressure (p_C) can be determined from the pressure versus volume data curve because, at this critical point B (as shown in Figure 4.3), debonding initiates and the volume is presumed to increase sharply and the pressure is presumed to drop accordingly. By substituting this critical pressure into equation(3.3.5), the analytical values of the adhesion strength in terms of strain energy release rates for the tested adhesive bonds can be obtained.

Experimental compliance method

In order to confirm our analytical solutions, the experimental compliance method was used to obtain the strain energy release rate, which is referred to as the experimental G value. This method was originally utilized in a blister

test for measuring the adhesion of paints and varnishes by Dannenburg[11]. In his blister test, Dannenburg measured the variation of the total work done by the external pressure system, δW. This work was equal to the energy required to debond the film, $G \cdot \delta A$, plus the variation of strain energy in stretching the film, δU, assuming that no plastic deformation takes place. δA is the increment in debonded area. The energy balance equation for this case is

$$\delta W = G_c \cdot \delta A + \delta U \qquad (4.1)$$

The last term δU in the above equation can be obtained either by performing the same pressure-volume measurements on a film which is not bonded onto the substrate, as done in Dannenburg's blister test, or by unloading the sample. The bond strength in terms of the strain energy release rate, G_C, can be determined as

$$G_c = \frac{\delta W - \delta U}{\delta A} \qquad (4.2)$$

In Figure 4.3, the variation of the total work done by the external pressure system, δW, equals to the area under curve 1 and 2 from point A to C. The area under curve 3 from A to C equals the variation of strain energy used to stretch the film during the blister process, δU. The difference between these two areas, which is the shaded area in Figure 4.3, represents the total energy required to propagate the crack (debonding), and is also equal to the strain energy release rate multiplied by the total debond area, assuming no plastic deformation has taken place. Therefore, the strain energy release rate for

this adhesively bonded system can be obtained from the pressure - volume data curve.

If there is plastic deformations involved during the loading procedure, the curves will shift right, and the unloading curve will not go back to the original point, A, as stated in section 4.3(a). At present, no technique is available to determine the amount of plastic deformations involved in this case; the strain energy release rate value cannot be obtained by these two methods described above.

(c) Young's modulus measurement

In the unloading region (line 3), information about the mechanical properties of the film may be obtained. The pressure-volume relations predicted by the theoretical model for a non-prestressed membrane is given by Equation (3.3), which can be expressed as,

$$V = \frac{w^{\frac{7}{3}}}{6}\left[\frac{3p(1-\nu^2)}{Et}\right]^{\frac{1}{3}} \cdot L \qquad (4.3)$$

where, for this peninsula blister specimen, w represents the groove width (=2a), and L represents the groove length.

This suggests that the data could be fitted to the form,

$$V = C^* \cdot p^{\frac{1}{3}} \qquad (4.4)$$

where

$$C^* = \frac{(2a)^{\frac{7}{3}}}{6}\left[\frac{3(1-\nu^2)}{Et}\right]^{\frac{1}{3}} \cdot L \qquad (4.5)$$

C^* can be determined by a least-square regression of the unloading pressure-volume curve, i.e. line 3 in Figure 4.3.

Comparing to the constitutive equation given in [17],

$$p = \left(\frac{V}{C}\right)^n \qquad (4.6)$$

where, V is the generalized displacement, p is the generalized force, and C is the generalized compliance, it can be easily seen that the coefficient C^* in equation (4.4) is the same as the compliance C in equation (4.6) when n=3. Therefore, the desired modulus of the film can be calculated from the fitted compliance C^* as,

$$E = \frac{3(1-\nu^2)(2a)^7 \cdot L}{(6C^*)^3 \cdot t} \qquad (4.7)$$

CHAPTER 5 APPLICATION OF THE PENINSULA BLISTER TEST

This chapter demonstrates the application of the peninsula blister geometry to some specific adhesive bonding systems. The current study involved five typical systems to study the feasibility of this newly developed technique. Some of these adhesive systems were successfully tested using the peninsula blister specimen, while others were unsuccessful due to various reasons. Table 5.1 lists the material systems tested. Results of these tests will be described and discussed in this chapter.

5.1. PSA Tapes Bonded On Aluminum Substrate

The pressure sensitive adhesive (PSA) tapes tested in this study were produced by the 3M Company. These blue packing tapes were 6 inches (152.4mm) wide, 3.5 mil (0.089 mm) thick, and were composed of a polyester backing and rubber adhesive.

Plates of commercial aluminum were machined into the shape shown in Figure 2.1 to be employed as substrates. All the aluminum substrates used in this research were approximately 5 inch (127mm) in length, 2.25 inch (57.2mm) in width, and 0.5 inch (12.7mm) to 1 inch (25.4mm) in height. The peninsula widths (2a, 2b) and length (L) of the substrate used for this PSA tape /aluminum application are listed in the following table:

2a	2b	L
3/4 inch (19.1mm)	1/16 inch (1.59mm)	3.7 inch (94mm)

Surface preparation for the aluminum substrate consisted of grinding with 360-A grit sandpaper in a roll-grinder, overflow rinsing in cold water and solvent cleaning with either alcohol or acetone.

The PSA tapes were cut into 2.25 inch (57.2mm) by 5 inch (127mm) rectangular sheets, and pressed onto the substrate in the regions of the peninsula and the outer perimeter. Intensive care was taken to make the suspended film free of wrinkles and stretching so that the requirements of a membrane with neither prestress nor initial slack were fulfilled. The preparation and the testing were performed at room temperature. The applied pressure and the blister volume data were measured using the experimental apparatus and procedures outlined in chapter 4.

Figure 5.1 shows the debonding results (debond length versus debonding time at several fixed pressures) obtained with the PSA tapes and aluminum substrates. Figure 5.2 gives the pressure versus volume information during a typical loading - debonding - unloading cycle for a PSA tape/aluminum joint. These results indicate that, at a constant pressure, the debonding rate was relatively constant along the major portion of the peninsula. Therefore, one important characteristic of the peninsula blister specimen, i.e., a constant strain energy release rate along the peninsula length, could be inferred. It

TABLE 5.1 MATERIAL SYSTEMS INVESTIGATED IN THIS RESEARCH

series	blister adherend	adhesive	substrate	results
1	polyester	rubber (PSA)	Al substrate	worked well
2	polyimide	cyanoacrylate or epoxy	Al substrate	worked well
3	polyimide		Al substrate	unsucceed in fabricating
4	coating		Al sheet	succeed in fabricating haven't been tested
5	copper	PPS	Al or Cu substrate	large plastic deformation induced

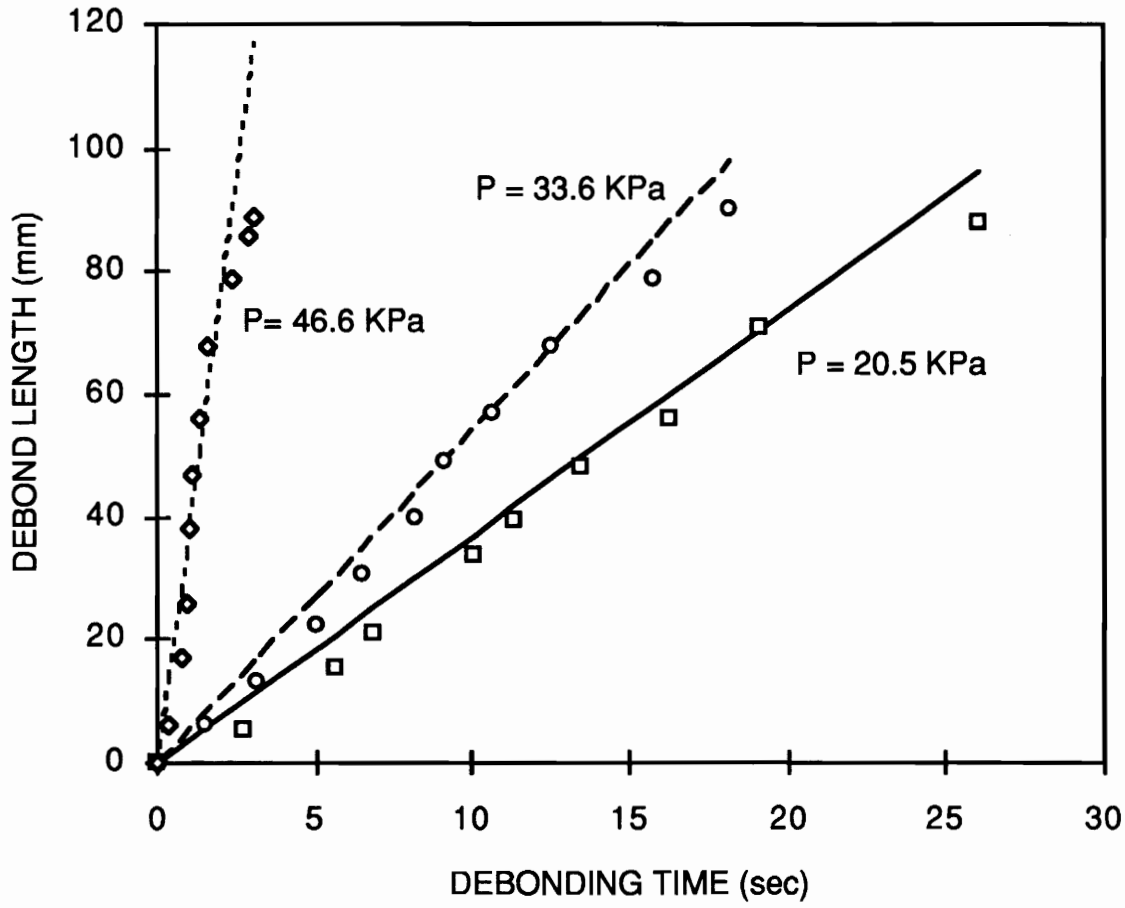

Figure 5.1 Debond Length versus Debonding Time For PSA Tapes bonded on Aluminum Substrate

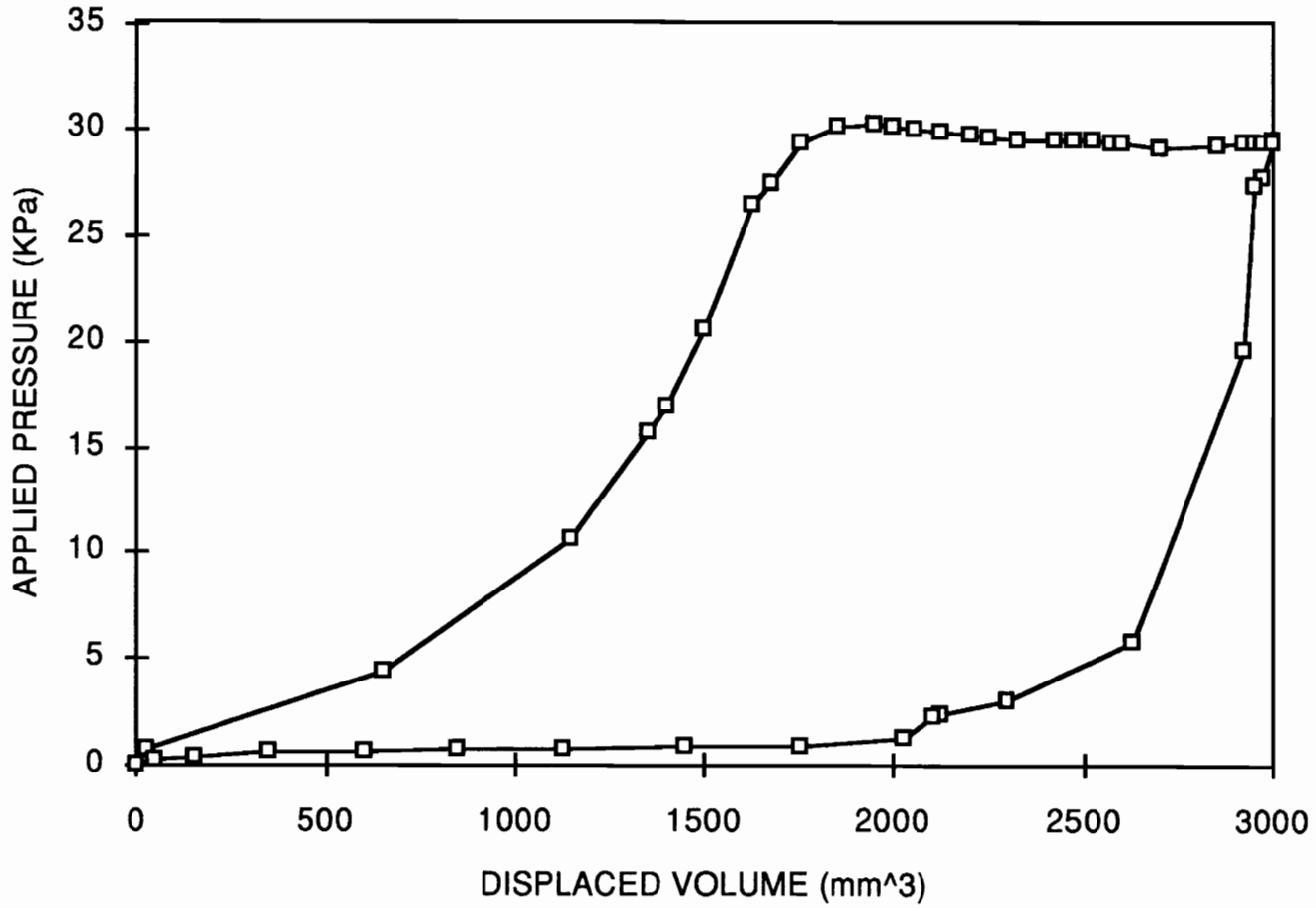

Figure 5.2 Typical Loading (debonding) and Unloading Curve for a PSA Tape Bonded on Aluminum Substrate

was also observed that debonding became slower near the end region of the specimen, where the strain energy release rates are known to decrease, according to Chapter 3 section 3.1.

As mentioned previously in Chapter 4, most of pressure sensitive adhesives are viscoelastic materials and exhibit significant time, temperature or loading rate dependent behavior. This viscoelastic behavior was studied using the peninsula blister tests. Chang, et. al [19], found that the creep of the polyester backing of this PSA tape was not significant, therefore, the viscoelastic behavior was present only in the pressure sensitive adhesives. At different pressures, debonding took place with different debonding rates. Figure 5.3 shows the dependence of the strain energy release rate on the debonding rate (G versus da/dt). The strain energy release rates here were calculated using the experimental compliance method described in section 4.3 based on pressure - volume curves of the tests. The theoretical solutions derived in Chapter 3 could not be employed in this case, because those solutions were all based on elastic theory, and haven't taken the viscoelastic dissipation into account.

To compare with these peninsula blister test results, peel tests at two different take-off angles (90^{o} and 180^{o}) were conducted for the same PSA tape / aluminum joints with a slip/peel tester, Model 3M90 of Instrumentor, Inc.. Results were also plotted in Figure 5.3. The comparison indicates that the test results from peninsula blister tests agreed fairly well with those from the peel tests.

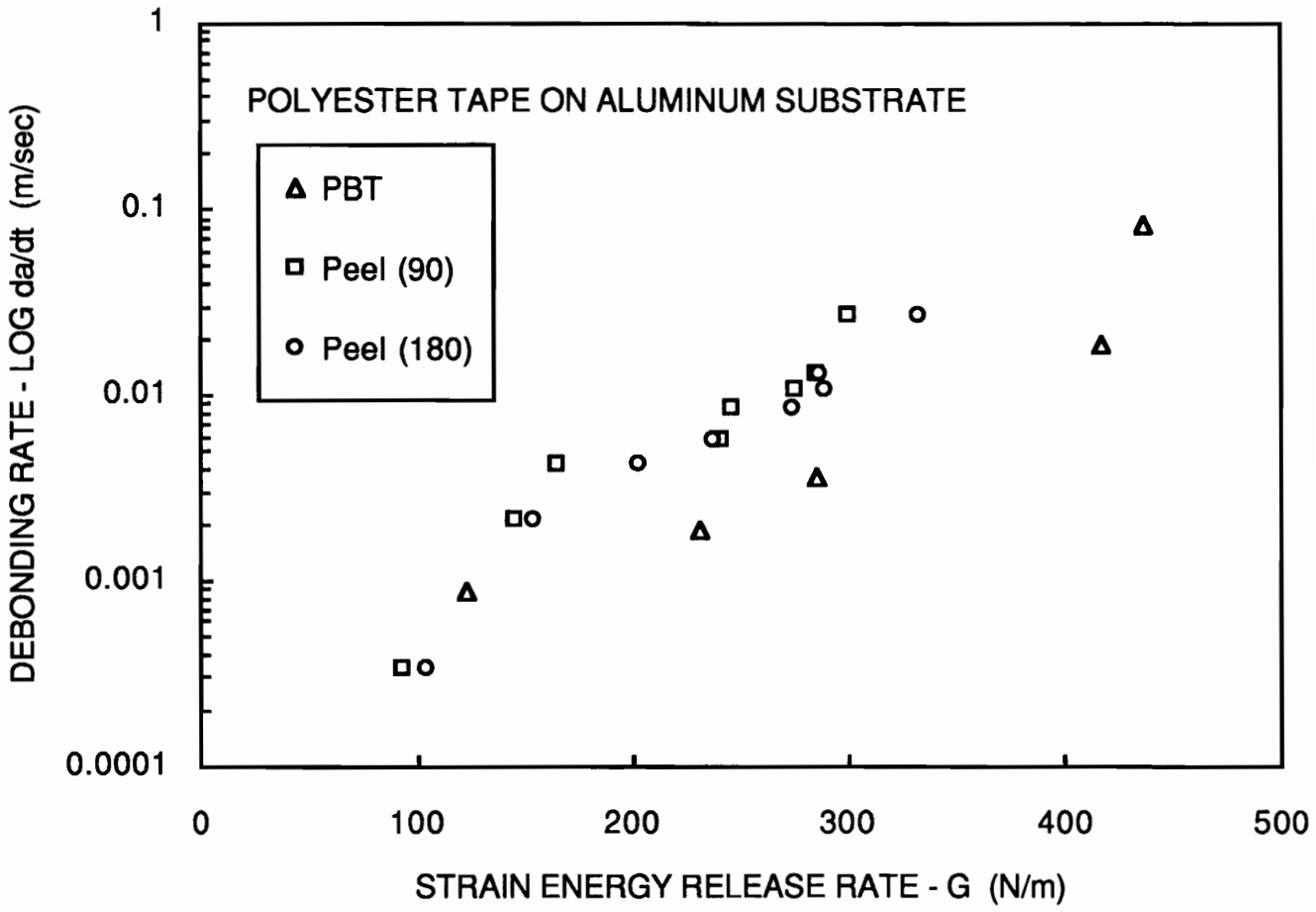

Figure 5.3 Effect of debonding rate on G for a PSA tape on aluminum substrate

Incidentally, it was also observed from the experiments that tapes were seriously curled after these large take-off angle peel tests, but less deformed after peninsula blister tests. The reason could be attributed to the fact that the peel angles in the peninsula blister tests were much smaller than the take-off angles of those peel tests, hence the bending effects in peninsula blister specimens were lower. Smaller take-off angles (or same peel angles as in peninsula blister tests) peel tests haven't been carried out in this study due to the limitations of equipments.

5.2. Polyimide Film and Aluminum Bonded with Cyanoacrylate or Epoxy

Two types of polyimide films were used in these adhesive joints. One was a 3 mil (0.076mm) thick film obtained from the E.I. Dupont de Nemours Corporation under the trade name Kapton® 300HN. The other polyimide film was produced by ICI as 1 mil (0.025mm) thick film, under the trade name of Upilex® S. Prior to bonding, surface preparation of these films involved alcohol cleaning.

The substrates used for this application were made of the same aluminum as used in the PSA tape / aluminum bonding systems. The peninsula widths (a, b) and length (L) of these substrates are listed in the following table

Substrate	2a	2b	L
#1	3/4 inch (19.1mm)	1/16 inch (1.59mm)	3.7 inch (94mm)
#2	0.8 inch (20.3mm)	0.05 inch (1.27mm)	3.7 inch (94mm)

The cyanoacrylate adhesive used in this study was obtained from Loctite Corporation, while the Two Ton® clear epoxy was commercially manufactured by Devcon Corporation. Cyanoacrylate is a fast-curing and strongly-adhering adhesive. Its curing agent is moisture. The two-part thermoset epoxy (consisting of epoxy resin and hardner) used in this study came in separate tubes, and was mixed thoroughly before bonding.

The polyimide films were cut into 2.25 inch (57.1mm) by 5 inch (127mm) rectangular sheets. Selected adhesives (cyanoacrylate adhesive or epoxy) were applied onto the bond area of the substrate, including the peninsula and the outer perimeter of the substrate. Then, the films were bonded onto the substrate under a weight pressure of approximately 5.55 KPa. When applying the adhesives onto the bonding area, care should be taken because an excessive or deficient amount of adhesive might cause serious edge spew or voids, respectively. Intensive care should also be taken to make the suspended film free of wrinkles and stretching so that the requirements of a membrane with neither prestress nor initial slack would be fulfilled. The initial debond was formed by placing a tiny drop of release agent at the tip of the peninsula before the adhesive was applied. The release agent used here was BUEHLER® Release Agent (No. 20-8185-008), manufactured by Buehler. The adhesives used in this phase of the research were cured at room temperature.

Since the cyanoacrylate and epoxy used herein were brittle materials, the mechanical and fracture behaviors of these adhesive joints were essentially elastic, and different debonding behaviors from PSA tapes were observed. Figure 5.4 is a typical loading and unloading curve for a polyimide film on an aluminum substrate with cyanoacrylate adhesive as the bonding agent. It was observed that debonding started at a critical pressure and propagated rapidly along the peninsula length till fully debonded. Because of the rapid debonding growth, only a very limited number of data points could be collected during the debond process by the data acquisition system.

Two tests with the same materials but different debond length were conducted, and the critical pressures were 6.11 psi (42.1 KPa) and 5.93 psi (40.9 KPa), respectively. One may also infer, from the agreement of these two critical pressures, the independence of the strain energy release rates on the debond length in the peninsula blister specimen.

Table 5.2 compares the G values obtained from both the theoretical analysis and the experimental compliance method for the two types of polyimide films mentioned above. The results have been divided into groups by horizontal lines. Each group represents strain energy release rate data of average values and standard deviations computed from tests with the same material joints and similar surface preparation. It was observed that the agreement of the data in a single group was fairly good, and the differences between theoretical and experimental results ranged approximately from 6% to 30%.

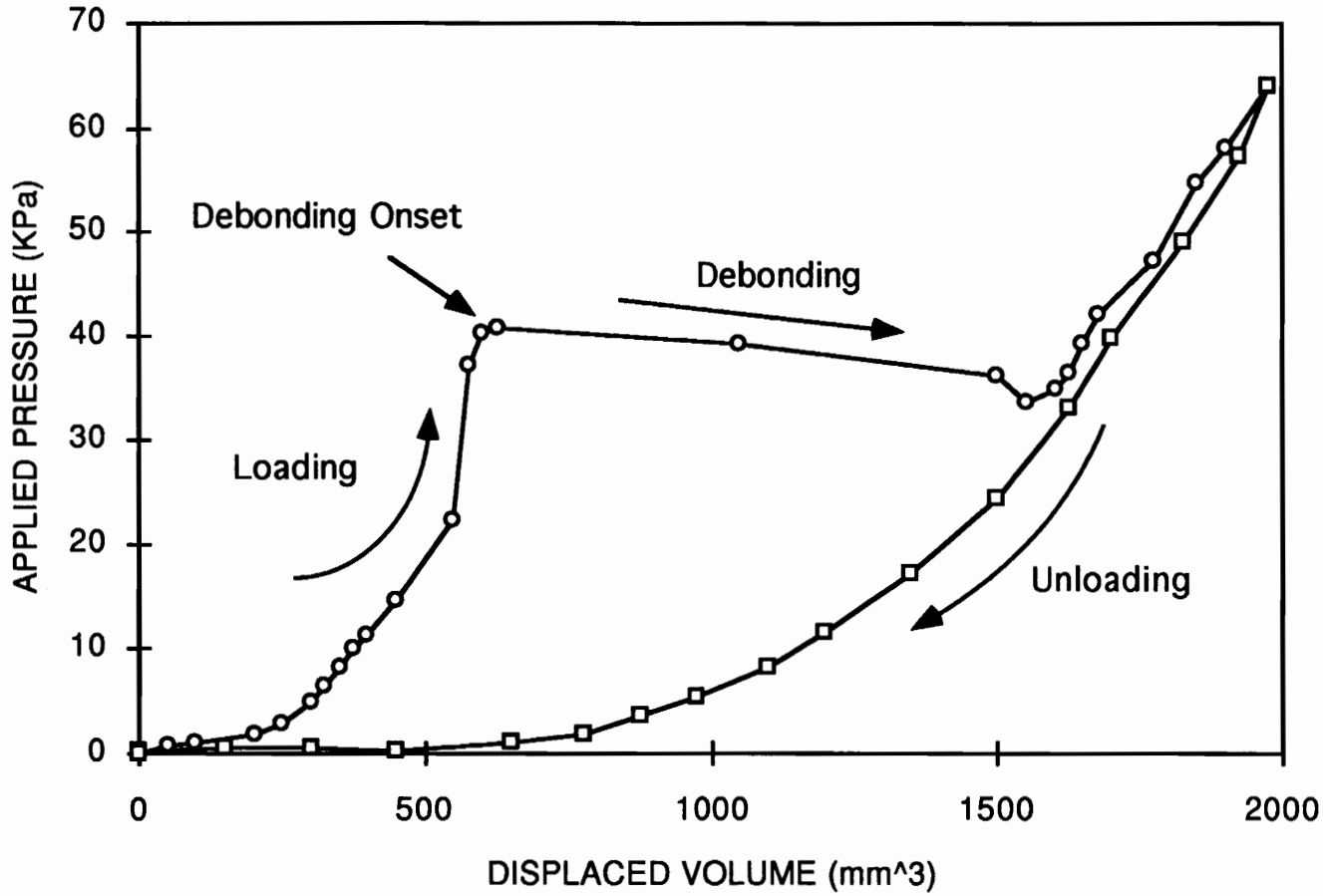

Figure 5.4 Typical Loading (debonding) and Unloading Curve for a Polyimide Film Bonded on Aluminum substrate

TABLE 5.2 ADHESION MEASUREMENT OF THIN POLYIMIDE FILMS ON ALUMINUM SUBSTRATES

Film (thickness)	Adhesive	Preparation (cure time)	G(J/m^2) (analysis)	G(J/m^2) (pV curve)
UPILEX ($2.5X10^{-2}$mm)	Cyanoacrylate	Alcohol clean (24 hours)	88.2	103.8
UPILEX ($2.5X10^{-2}$mm)	Cyanoacrylate	Alcohol clean (24 hours)	77.7	84.9
KAPTON ($7.6X10^{-2}$mm)	Cyanoacrylate	Acetone clean (24 hours)	266	294
KAPTON ($7.6X10^{-2}$mm)	Cyanoacrylate	Acetone clean (1 hour)	124	178
KAPTON ($7.6X10^{-2}$mm)	Epoxy	Acetone clean (1 hour)	127.5	135
KAPTON ($7.6X10^{-2}$mm)	Epoxy	Acetone clean (1 hour)	126.8	135
KAPTON ($7.6X10^{-2}$mm)	Cyanoacrylate	Acetone clean (1 hour)	111.2	115
KAPTON ($7.6X10^{-2}$mm)	Cyanoacrylate	Acetone clean (1 hour)	110.6	115

One may also observe from the above results that the G values obtained from pressure - volume curves were always larger than those from the theoretical analysis. These differences could be caused by the following reasons:

(1) According to the error analysis at the end of Chapter 3.3, the predicted (theoretical) strain energy release rates are based on the assumptions of small deformation. If the blister deflections were not small enough, the calculated membrane strains would be smaller than the true membrane strain values, which led to the values of the predicted strain energy release rates smaller than the true values of the strain energy release rates.

(2) The theoretical values of strain energy release rates (predicted values) were obtained from single points, while the experimental values of G were from the averages of the entire debonding region, which included the end regions where strain energy release rates were lower. Thus, the experimental G were larger than theoretical ones. This phase of error could be overcome by taking p-v data over a narrow range of peninsula length.

(3) If there was a small amount of initial slack existed in the film, film stretching will be less. The true values of strain energy variation would be less than that for non-initial-slack films. Therefore, if we still applied the equations derived from a non-initial-slack case, the predicted strain energy release rates would be smaller than the true values.

For comparison purposes, standard blister tests (initial blister radius 13.5mm) and 90^{o} peel tests (12.7 mm wide) were also performed on the same adhesive joints and with the same surface preparation as used with the peninsula blister test. Results are listed in Table 5.3. These results are divided into three groups by vertical lines. Each group represents strain energy release rate data obtained from different test methods on the same adhesive bonding system, i.e., polyimide films bonded to an aluminum substrate with cyanoacrylate adhesive.

It was also observed that films often failed in the peel tests, but no film rupture occurred in the peninsula blister tests for the material systems used in this research. Once again, the reason may be attributed to the fact that the peel angles in the peninsula blister tests were much smaller than the take-off angles (90^{o}) of those peel tests, hence the bending effects in peninsula blister specimens were lower. Smaller take-off angles peel tests haven't been carried out in this research due to the limitations of equipment.

In order to demonstrate that no plastic deformation of the blister adherends occurred during testing, multiple pressure - volume measurements were carried out on a same debonded polyimide film. If plastic deformations had taken place, the two pressure-volume curves would not be reproducible. Figure 5.5 shows typical behavior of two consecutive p-v measurements on the same polyimide film. As can be seen, the two sets of data are nearly identical.

TABLE 5.3 COMPARISON OF THE ADHESION MEASUREMENT BY DIFFERENT TEST METHODS

(Polyimide film bonded on aluminum substrate by cyanoacrylate adhesive)

Test Method	Peel Test		Standard Blister	Peninsula Blister	
Film Thickness (mm)	$2.5X10^{-2}$	$7.6X10^{-2}$	$2.5X10^{-2}$	$2.5X10^{-2}$	$2.5X10^{-2}$
Peeling Force or Debonding Pressure	1.186(N)	1.245(N)	$6.52x10^{4}$(Pa)	$4.21x10^{4}$(Pa)	$6.07x10^{4}$(Pa)
Dimensions (mm)	w = 10.4	w = 11.43	2 r = 25.4	2a = 50.8 2b = 1.59	2a = 50.8 2b = 1.59
Adhesion Strength G (J/m^2)	113±24	119±4	76	83±7.4	124

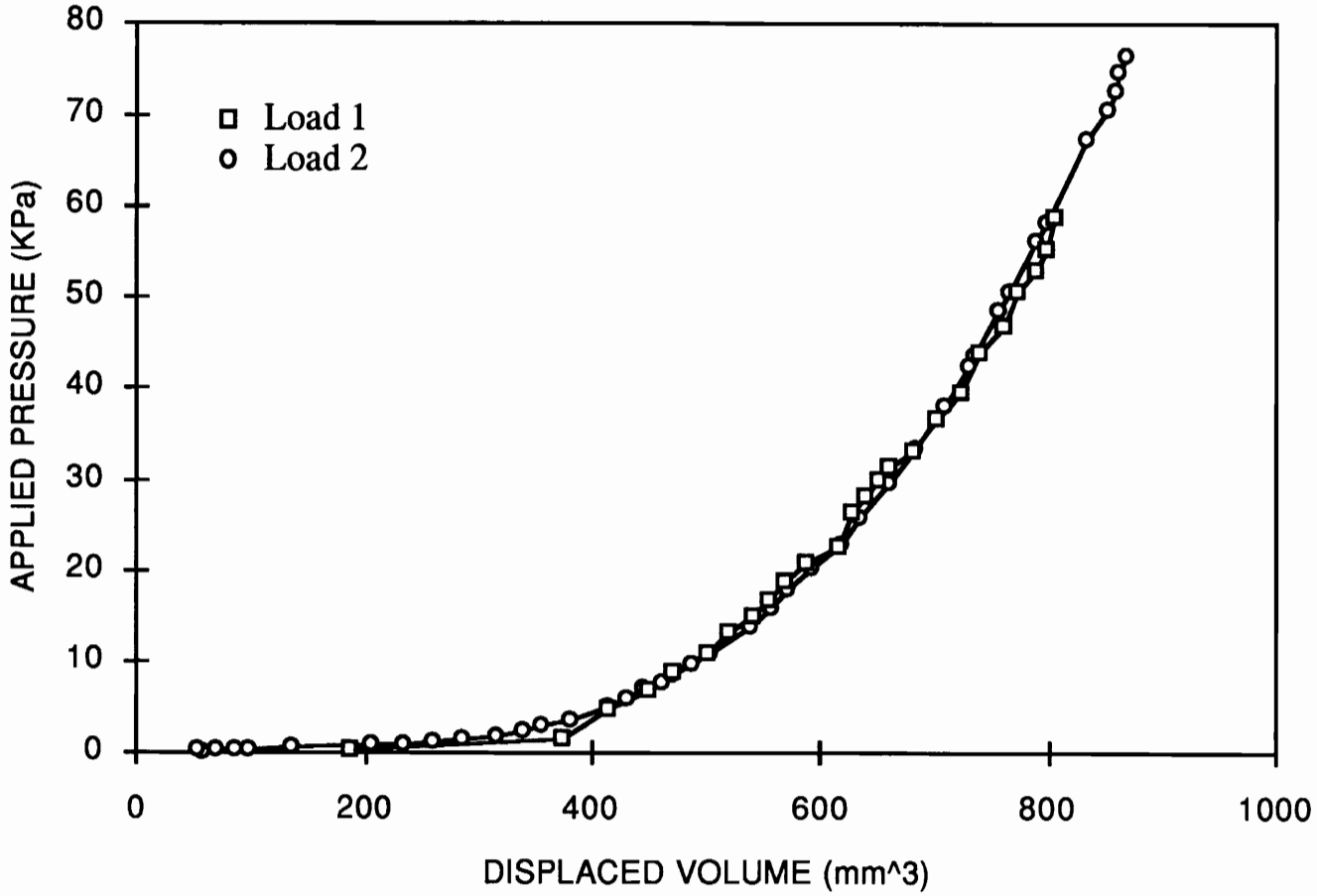

Figure 5.5 Consecutive Loading and Unloading Curve for a Peeled Polyimide Film

5.3. Measurement of Young's Modulus

As analyzed in Chapter 4, section 4.3, the Young's modulus of the film can also be extracted based on the best fit line drawn through the pressure-volume data points acquired from peeled films. This was accomplished by importing the data files containing pressure and volume data points of a peeled film and the values of the specimen dimensions a and t, into the Excel 3.0 software package. The Poisson's ratio used here was 0.34 as given by the industry literature and was not verified in this work. The coefficients, i.e., the compliance C^*, could then be calculated using standard least-square fitting techniques. From these coefficients, the values of E were resolved by equation (4.7). It is noteworthy that the theoretical model predicted in Chapter 3 could also be checked and verified by this fitting technique.

Table 5.4 presents the Young's modulus data acquired from polyimide films of different thicknesses from the peninsula blister tests. The results are also divided into groups by horizontal lines. Each group represents data from a single processing batch. The Young's modulus data listed in the manufacturer's industry literature for Kapton® 300HN (1 mil) and Upilex® S (1 mil) are 2.55 GPa and 8.8 GPa, respectively. For comparison, tensile tests had also been conducted on Polymer Laboratory Minimat (miniature loading frame), and the modulus data of these two types of polyimide films acquired from these tensile tests were 2.2 GPa and 5.8 GPa, respectively. As can be seen, agreement is fairly good throughout the experimental range, and the values calculated for E from the peninsula blister tests are of the correct order of magnitude.

TABLE 5.4 MEASUREMENT OF YOUNG'S MODULUS BY PENINSULA BLISTER SPECIMEN

Film	Thickness	Substrate dimensions	Compliance C^*	Young's Modulus
Kapton	0.076 (mm)	2a = 12.7 mm	328.4	1.66 GPa
		L = 113.5 mm	317.6	1.83 GPa
		2a = 19 mm	931.0	1.80 GPa
		L = 113 mm	980.0	1.50 GPa
Upilex	0.025 (mm)	2a = 12 mm	462.9	1.80 GPa
		L = 113.5 mm	443.7	2.01 GPa
		2a = 19 mm	1658.92	0.95 GPa
		L = 113 mm		

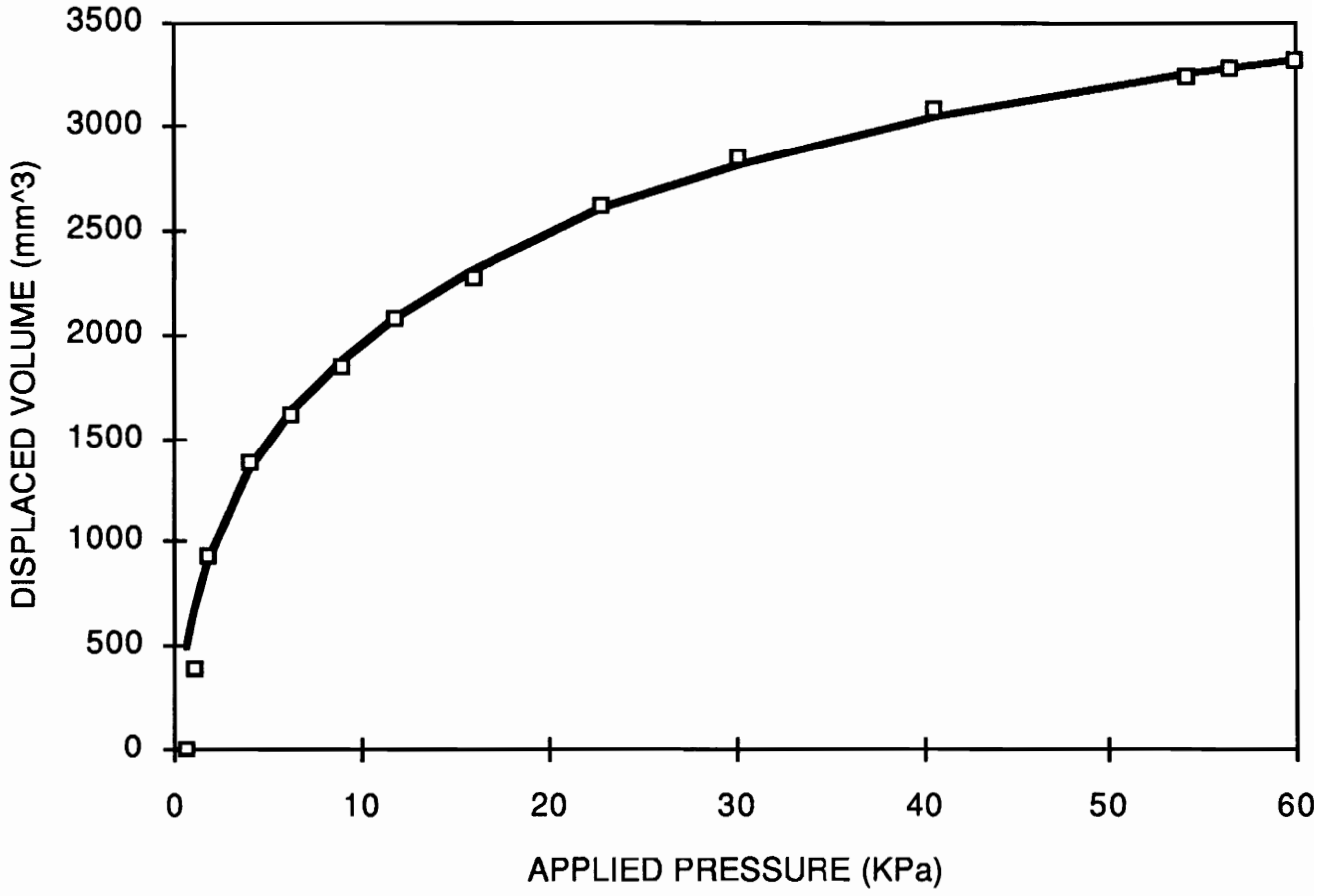

Figure 5.6 Fitting of an Unloading Curve for a Peeled Polyimide Film

Figure 5.6 shows a typical graph of the pressure-volume data and a fitting curve through the data points from a 1 mil (0.025 mm) polyimide film. Plots of the other data are very similar to Figure 4.9 except the curvatures. The generalized compliance C* in equation (4.4) and (4.5) represents the curvature of the pressure-volume curve. From Table 5.4, one could also see that, the compliances become larger when the substrate widths are larger or the film thicknesses are smaller.

5.4. Polyimide Coatings on Metal Substrate

The adhesion between coatings and substrates are always of great interest and importance to researchers and manufacturers. As stated in the introduction, when testing the adhesion of coatings, blister tests are favored due to the nature of uniform pressurizing and less film stretching. Polymer coatings are usually coated onto the substrates by either solvent casting or spin coating from solution. Thus, problems have been encountered on how to fabricate a suspended coating film onto a blister substrate with a central hole. This becomes more difficult for modified blister specimens, such as island and the peninsula blister specimens, which have more complicated initial debonds.

Hinkley [14] succeeded in fabricating a suspended polymer coating on a silicon wafer and forming a standard blister site by using an etching solution of HF and HNO_3 mixture. Allen and Senturia [21, 22] developed the island blister test and fabricated thin polyimide films on silicon wafer substrates by a photolithographic etching technique. The island blister test was also utilized

to study the adhesion of polyimide / metal interface. Although they succeeded in forming a polyimide / metal interface onto the island substrate, it should be noted that the metals (aluminum, chromium and titanium) in their tests were deposited in an electron beam evaporator. Therefore, the interface of their polyimide / metal were not the same as that of polyimide coated onto a metal substrate, because the interface in the second case involved metal oxide while the first one didn't.

In the application of the peninsula blister technique, efforts have been made to fabricate suspended polyimide coatings on an aluminum peninsula substrate. A hollowed peninsula substrate (as shown in Figure 5.7(a)) was designed specially for this purpose. A polyamic acid solution in diglyme (30%) was used as the coating material, and wax was employed as a filler. Prior to coating, a flat paper-backing adhesive tape was bonded onto the testing side of the substrate, thus a groove was formed to be partly filled with wax. By melting the wax and then cooling down to room temperature, a flat surface was formed on the testing side of the substrate. The polyamic acid solution was then spin-coated onto this flat surface after the removal of the adhesive tape. It was postulated that a thin coating could be formed after the solvent was evaporated in an air circulating chamber at room temperature. Then the wax could be removed by heating to 70^{o}C. Finally, the imidization of the polymer coating could be carried out by heating to 300^{o}C, holding for 30 minutes and then cooling down to room temperature in an air circulating oven. This procedure is depicted in Figure 5.7.

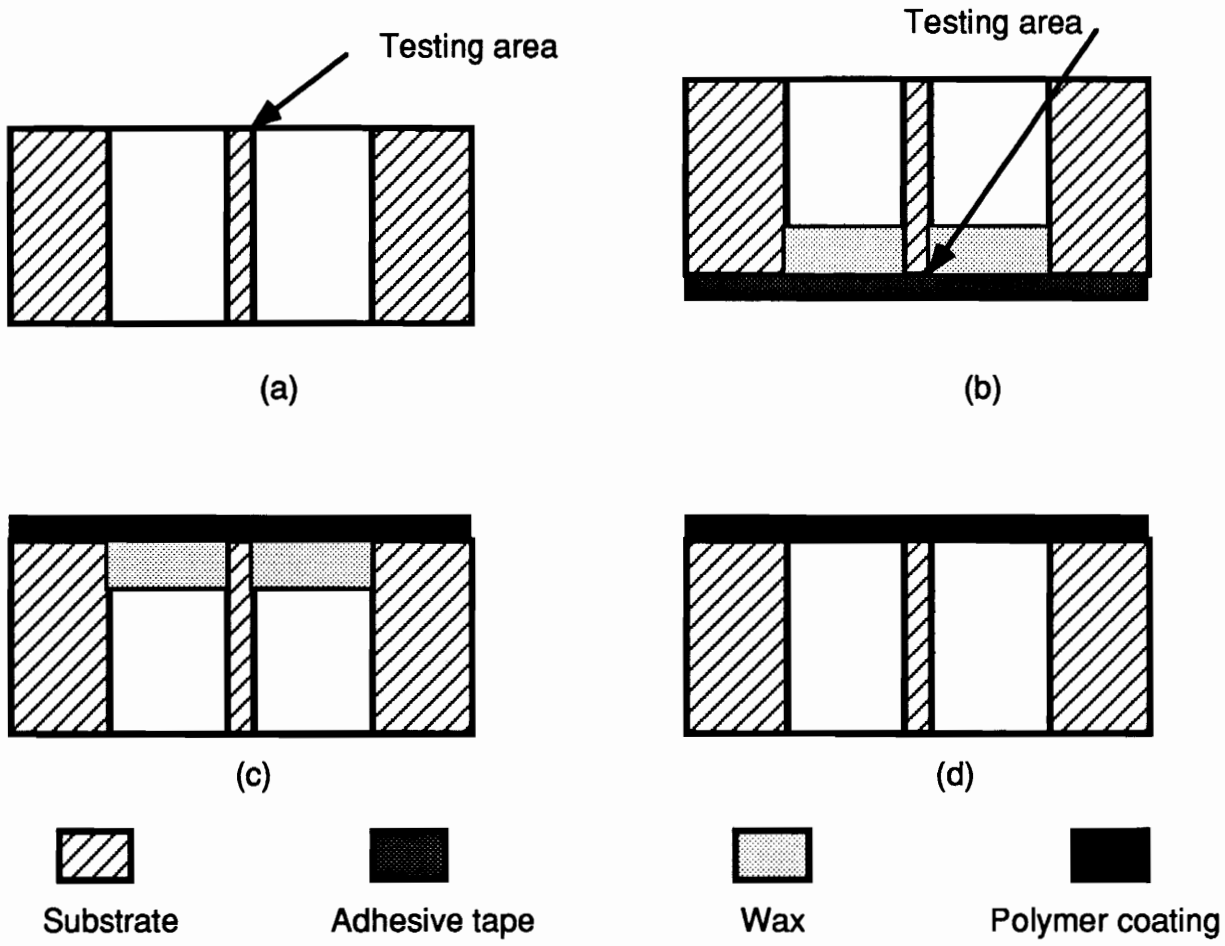

Figure 5.7 Desired Procedure to Form a Polymer Coating on Peninsula Substrate

It was presumed that the filler material (wax) would not be dissolved by the solvent diglyme. However, in actual practice, it was observed that the top part of the wax (or the impurities of the wax) was dissolved by the solvent resulting in a third material instead of polyimide coating on the surface of the substrate. Polyethylene glycol was also employed as filler due to the water soluble nature, but was also dissolved by the solvent. Even so, it was believed that this fabrication method was still practicable if an appropriate filler material is available. One suggestion made was to use one of the low melting point metals, such as wood's metal. Due to the time limitation, this application was not continued further.

5.5. Polymer Coating on Aluminum Sheets

One of the most interesting adhesion problem we would eventually like to study is the adhesion of polymer coatings on aluminum sheets, such as used in the soft drink industry. The samples used in this study were supplied by the technical center of Aluminum Company of America (ALCOA). The two samples were 10 mil (0.25mm) thick aluminum sheet coated (8 - 10 mm thick) with an epoxy-based electrocoat formulation, and a PVC-based roll-coat formulation, respectively. Efforts have been made to etch away a U-shaped region in the aluminum sheet, thus forming a suspended coating on the aluminum sheet. Details of the etching procedures can be found in Appendix B and Figure 5.8(a). After etching, the sample would be bonded onto a peninsula substrate for testing, as depicted in Figure 5.8(a). The sheet samples were successfully etched into the desired shape, but haven't been tested due to time limitation.

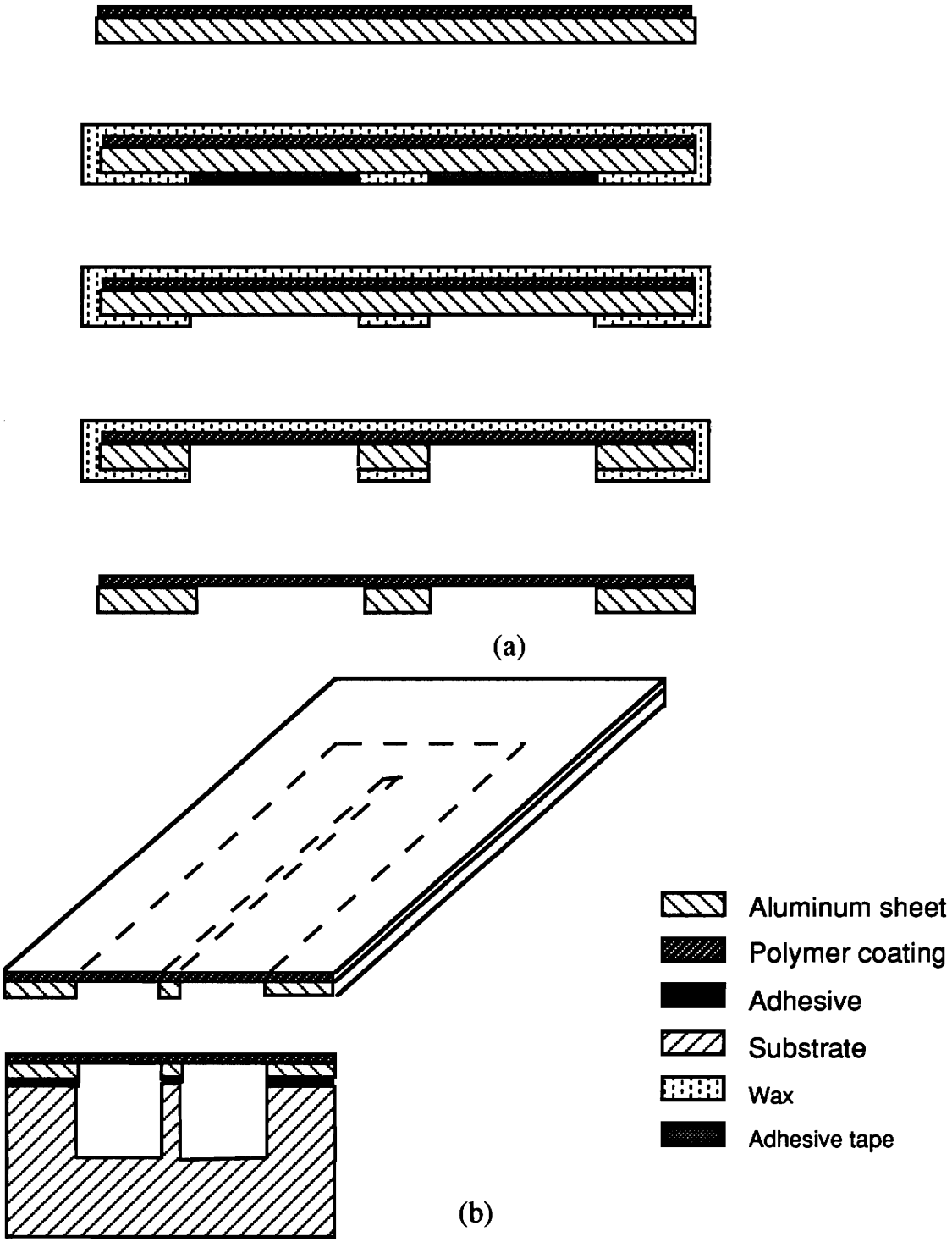

Figure 5.8 Desired Procedure to Etch Coating / Aluminum Sheets and Fabricate Peninsula Blister Specimen

The practical significance of this adhesion problem and the preliminary etching work in applying the peninsula blister technique make it worth investigating further.

5.6. Adhesion of Copper Films and PPS Adhesive

Copper is among those groups of material that have weak adhesion to most of materials. One of the objectives of the research conducted by Webster and Phillips Petroleum Corp. was to develop bonding techniques to increase the adhesion of the copper/polyphenylene sulfide (PPS) interface. In order to quantitatively evaluate the adhesion of this specific interface, peninsula blister tests were conducted. Fabrication of this system was similar to that of the material joints detailed in section 5.2. PPS film was compressed between copper foil and the substrate (aluminum or copper) at a temperature of 300^{o}C. In the cases of Cu/PPS/Al joints, failure can be ensured between Cu/PPS substrate. After the samples were bonded, it was observed that large amount of wrinkles was produced in the Cu/PPS/Al joints, while no significant wrinkles existed in the Cu/PPS/Cu joints. The reason could be attributed to the differences of the thermal-expansion coefficients of copper, aluminum and PPS.

The peninsula blister tests were performed for the Cu/PPS/Cu joints. Typical loading-debonding-unloading data are shown in Figure 5.9. From both the peeled specimen and the recorded pressure - volume data shown in Figure 5.9, a large amount of plastic deformation was observed to have taken place during the loading procedure. The interpretation of the data to adhesion strength

measurement for this case couldn't been carried out, since no analytical solutions are available for this nonlinear behavior.

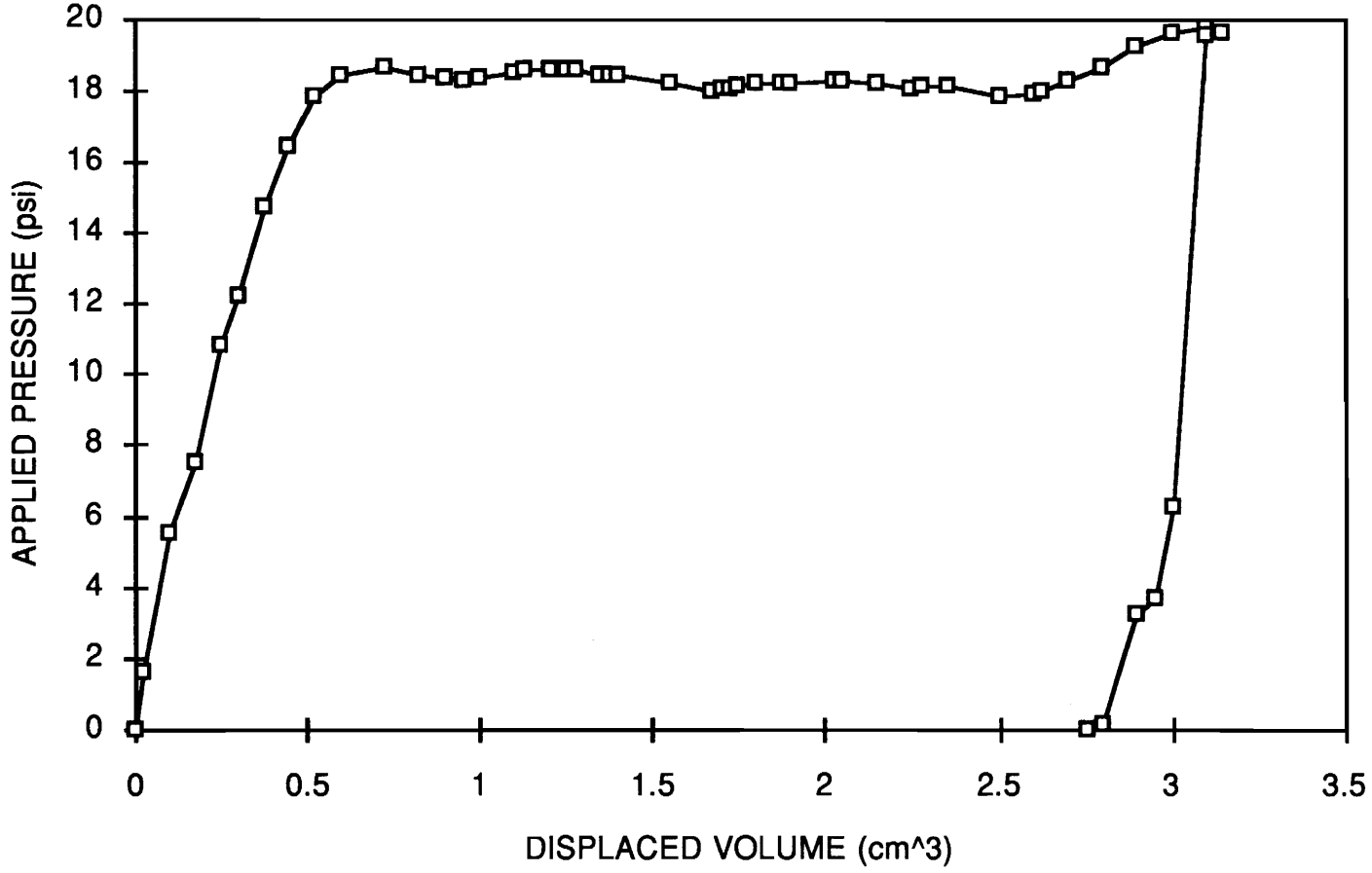

Figure 5.9 Typical Loading, Debonding and Unloading Curve for Cu/PPS/Cu Joints

CHAPTER 6 SUMMARY AND CONCLUSIONS

6.1 Summary

The work accomplished in this research can be summarized into three major parts; analytical modeling, development of the experimental technique and some applications of this developed technique. Each part will be briefly summarized below.

In the analytical part of this study, closed form solutions have been derived to predict the strain energy release rates for a plate adherend, a prestressed membrane adherend, a non-prestressed membrane adherend and a membrane adherend with initial slack. These solutions reveal that truly constant strain energy release rates can be produced along the major portion of the peninsula. Efforts have also been made in analyzing the stress status of the blister adherends for non-prestressed membrane case with several thin film adhesion test specimens in order to understand if film rupture can be reduced by geometry modifications. Although no solid conclusions can be made at the present time, primary studies indicate that this specimen, as well as the island blister specimen, may not be as good as we expected. High ratio of strain energy release rate to applied pressure cannot overcome the tensile strength limitations in thin film adhesion measurements. Whether the tensile strength limitation can be overcome by modifying blister geometries is still questionable.

An experimental technique and testing procedure have been established for adhesion measurements of thin film adhesive joints. Two methods have been used to calculate the strain energy release rates from the pressure - volume data acquired; an analytical method and an experimental compliance method.

Several material systems have been tested using this technique. Results of PSA tape / aluminum bonded joints suggest that debonding proceeds at constant rate under a constant pressure, while the results from polyimide / adhesive / aluminum joints show that critical pressures are independent of debonding length. Both of these results reveal that constant strain energy release rates can be produced in this specimen. In the second case, the good agreement of the strain energy release rate values obtained from the theoretical solutions and the experimental methods indicates the feasibility of this technique. Although we would like to test the adhesion of well-adhered coatings, the fabrication of the polyimide/metal joint into a peninsula blister site have not been completed due to material and time limitations. For adhesive bonding systems where large plastic deformations might take place, blister tests are not recommended to evaluate the adhesion strength since no analytical model is available either for this specimen or for other blister specimens.

6.2 Conclusion

In conclusion, a fracture test which can produce a high and constant strain energy release rate has been developed in this study. Although recent investigations on the stress analysis for various blister geometries suggests that the high strain energy release rate to applied pressure might not be able

to overcome tensile strength limitations for thin film measurement, the nature of truly constant strain energy release rate produced by this peninsula blister specimen still offers advantages over other blister tests. The agreement of the strain energy release rates obtained from both the experimental methods and theoretical solutions indicates the feasibility of this developed technique. Although problems still exist in fabricating and testing some adhesively bonding systems, the constant strain energy release rate nature of this peninsula blister specimen warrants further investigation and applications to wider and more versatile adhesion systems.

6.3 Recommendations For Future Work

Although most of the objectives were accomplished in this study, there are still some improvements which need to be made for future investigations. These include:

(1) As suggested in Chapter 3.5, there are still some unsolved problems, such as the stress distributions, associated with the island blister, constrained blister and the peninsula blister geometries. In order to better understand the mechanics and fracture behaviors with these modified blister geometries, it is necessary to develop numerical and analytical models to develop the relations of strain energy release rate, membrane stress and geometry factors for these blister geometries.

(2) In order to study the fracture behavior of more adhesive bonding systems under versatile loading conditions, an automatic control system

is needed to have better control of the flow rate or the applied pressures.

(3) Current work on coating adhesion suggests the need for further investigation in applying the peninsula blister specimen to the adhesion measurement of coatings.

(4) Mode mix of the peninsula specimen is an unsolved problem of this research. Finite Element Analysis is recommended for this study.

(5) XPS and contact angle measurements are two useful tools to experimentally investigate the failure modes by analyzing failed peninsula blister adherends and substrates.

REFERENCES

1) J. W. Obreimoff, "The Splitting Strength of Mica", *Proc. of the Royal Society of London*, A 127, 290-297 (1930).

2) E. J. Ripling, S. Mostovoy, and R. L. Patrick, *Mat. Res. Stand. MTRSA, ASTM*, 64(3), 129-134 (1964).

3) E. J. Ripling, S. Mostovoy, and H. T. Corten, "Fracture Mechanics: A Tool for Evaluating Structural Adhesives," *J. Adhesion*, 3, 107-123 (1971).

4) G. P. Anderson, S. J. Bennett, K. L. DeVries, *Analysis and Testing of Adhesive Bonds*, Academic Press, New York, New York, 1977.

5) J. O. Outwater and D. J. Gerry, "Fracture Energy, Rehealing Velocity, and Refracture Energy of Cast Epoxy Resins," *J Adhesion*, 72, 290-298 (1969).

6) T. R. Brussat, S. T. Chiu, and S. Mostovoy, "Fracture Mechanics for Structural Adhesive Bonds," *AFML-TR-163*, Air Force Materials Lab, Dayton, Ohio, (1977).

7) D. A. Dillard, John Z. Wang, " A Simple Constant Strain Energy Release Rate Loading Method for Double Cantilever Beam Specimens", presented at the 15th annual meeting of Adhesion Society, *J. of Adhesion* (in press), 1992

8) D. H. Kaelble, "Theory and Analysis of Peel Adhesion: Bond Stresses and Distributions", *Transactions of The Society of Reology*, 4, 45-73 (1960)

9) A. N. Gent and G. R. Hamed, "Peel Mechanics for an Elastic-Plastics Adherend", *J. Applied Polymer Science*, 21, 2817-2831 (1977)

10) K. Kendal, "Interfacial Cracking of Composite", *J. Material Science*, 11, 638 - 644 (1976).

11) H. Dannenberg, "Measurement of Adhesion by a Blister Method", *J. Applied Polymer Science*, 5, 125-134 (1961).

12) M.L.Williams,"The Continuum Interpretation for Fracture and Adhesion", *J. Applied Polymer Science*, 13, 29-40 (1969).

13) A. N. Gent and L. H. Lewandowski, "Blow-Off Pressures for Adhering Layers," *J. Applied Polymer Science*, 33, 1567-1577 (1987).

14) J. A. Hinkley, "A Blister Test for Adhesion of Polymer Films to SiO_2", *J. Adhesion*, 16, 115-126 (1983)

15) M. Fernando and A. J. Kinloch, "Use of the 'Inverted-Blister' Test to Study the Adhesion of Photopolymers", *Int. J. Adhesion and Adhesives*, April, 69-76 (1990)

16) K. R. Jiang, L. S. Penn, "Use of the Blister Test to Study the Adhesion of Brittle Materials", *J. Adhesion*, 32 (4), 203-226 (1990)

17) D. A. Dillard and Y. S. Chang, "The Constrained Blister--A Novel Constant Strain Energy Release Rate Test for Adhesives," *CASS/ESM-87-8*, Virginia Polytechnic Institute, Blacksburg, Virginia, Sept. 1987.

18) Y. S. Chang, Y. H. Lai, and D. A. Dillard, "The Constrained Blister -- A Nearly Constant Strain Energy Release Rate Test for Adhesives," *J. Adhesion*, 27, 197-211 (1989)

19) M. J. Napolitano, A. Chudnovsky, and A. Moet, "The Constrained Blister Test for the Energy of Interfacial Adhesion," *J. Adhesion Science and Technology*, 2 (4), 311-323 (1988)

20) Y. H. Lai and D. A. Dillard, "An Analytical Solution for the Constrained Blister Test Geometry," *J. of Adhesion*, 31, 177-189 (1990)

21) M. G. Allen and S. D. Senturia, "Analysis of Critical Debonding Pressures of Stressed Thin Film in the Blister Test," *J. Adhesion*, 25, 303-315 (1988).

23) D. A. Dillard, Y. H. Lai, Y. S. Chang, T. Corson, and Y. Bao, "Alternate Blister Geometries for Measuring the Fracture Toughness of Adhesive Bonds", *Proc. 1990 SEM Conference on Experimental Mechanics*, Albuquerque, NM, June 1990.

24) D. A. Dillard and Y. Bao, "The Peninsula Blister Test: A High and Constant Strain Energy Release Rate Fracture Specimen for Adhesives", *J. Adhesion*, 33, 253-271 (1991)

25) Y. Bao and D. A. Dillard, "Application of the Peninsula Blister Specimen to the Adhesion Measurement of thin Polymer Film", *Proc. 15th. Annual Meeting of Adhesion Society*, Hilton Head, SC, February, 1992

26) S.Timoshenko and S. Woinowsky-Krieger, *Theory of Plates and Shells*, Second Edition, McGraw-Hill, New York, 1959.

27) MACSYMA, Computer Softer, Symbolics, Inc., 1986.

28) M. G. Allen, "Measurement of Adhesion and Mechanical Properties of Thin Films Using Microfabricated Structures", *PhD. Dissertation*, MIT, Boston, MA, 1989

29) Y. H. Lai, personal communication, May, 1992.

APPENDIX A. PLATE SOLUTION FOR ISLAND BLISTER SPECIMEN

For the island blister, we can assume that the deflections of the blister adherend do not exceed the order of the thickness of the blister adherend. So, simple plate theory can be applied, and the governing equation can be expressed as:

$$\nabla^4\omega=-\frac{p}{D} \qquad (1)$$

The deflection is given as:

$$\omega(r)=C_1+C_2\cdot\ln r+C_3\cdot r^2+C_4\cdot r^2\cdot\ln r+\frac{pr^4}{64D} \qquad (2)$$

For the case of an island blister, four boundary conditions are applied at the debond edge of the island (b), and the outer radius (a),

$$\omega(b)=0, \qquad \frac{d\omega(a)}{dr}=0 \qquad (3a)$$

$$\omega(a)=0, \qquad \frac{d\omega(a)}{dr}=0 \qquad (3b)$$

The closed form solution was obtained using MACSYMA [27]:

$$C_1=\frac{p}{64D}\cdot\frac{4a^2b^2(b^4\ln a-a^4\ln b)(\ln a-\ln b)+a^2b^2(a^2-b^2)^2[2(\ln a+\ln b)-1]}{[2ab(\ln a-\ln b)]^2-(a^2-b^2)^2} \quad (4a)$$

$$C_2=\frac{p}{16D}\cdot\frac{a^2b^2(b^4-a^4)(\ln b-\ln a)-a^2b^2(a^4+b^4)^2+2a^4b^4}{[2ab(\ln a-\ln b)]^2-(a^2-b^2)^2} \quad (4b)$$

$$C_3=\frac{p}{64D}\cdot\frac{8a^2b^2[(b\ln a)^2+(a\ln b)^2-(a^2+b^2)(\ln a\cdot\ln b)+(a^2-b^2)^2[a^2(2\ln a-1)+b^2(2\ln b-1)]}{[2ab(\ln a-\ln b)]^2-(a^2-b^2)^2} \quad (4c)$$

$$C_4=\frac{p}{32D}\cdot\frac{(a^2-b^2)[a^4-b^4-4a^2b^2(\ln a-\ln b)]}{[2ab(\ln a-\ln b)]^2-(a^2-b^2)^2} \quad (4d)$$

Substituting these expressions into equation (2) and then integrating with respect to debond area, we can obtain the compliance:

$$C=\frac{2\pi}{p}\int_b^a\omega(r)\cdot r\,dr$$

$$=\frac{\pi}{2p}\left[\frac{p(a^6-b^6)}{96D}+C_4\frac{4(a^4\ln a-b^4\ln b)-(a^4-b^4)}{4}+C_3(a^4-b^4)+C_2(2a^2\ln a-2b^2\ln b-a^2+b^2)+2C_1(a^2-b^2)\right] \quad (5)$$

Applying Equation (2.1), the strain energy release rate may be found from:

$$G=\frac{1}{2}p^2\frac{\partial C}{\partial A}=\frac{p^2}{4\pi}\cdot\frac{\partial C}{\partial b} \quad (6)$$

APPENDIX B. ETCHING PROCEDURE FOR COATINGS AND ALUMINUM SHEET BONDS

(1) Cut the aluminum sheet sample into rectangular shape of desired size.

(2) Gently rub the non-coated side of the sample using a small piece of sandpaper, followed by cold water rinsing.

(3) Cut a strip of adhesive tape into an U-shape to cover the areas needs to be etched away and bonded onto the rubbed side of the aluminum sample sheet.

(4) Melt the wax in a flask at around 60^{o}C, and then soak the sheet sample into this flask for a few seconds. Take the sample out to solidify the wax after the whole sheet is coated with wax.

(4) Carefully tear away the adhesive tape from the sheet sample so that the area that needs to be etched away exposed to the air.

(5) Put the sheet sample into sodium hydroxide solution (20%wt) at room temperature and start etching. It is preferred to have a magnetic stir-bar in the NaoH container and a stir plate under the flask in order to accelerate the etching procedure. For the aluminum sheet samples tested in this research this etching procedure takes approximately one hour in 20% (wt) solution.

VITA

The author, Yong Bao, was born on Oct. 2, 1964 in Shangrao, Jiangxi Province, People's Republic of China. In 1972, she moved with her parents to Maanshan, Anhui Province, where she received her elementary education from primary school, middle school and high school. In September of 1982, she entered the University of Science and Technology of China. After graduating in June, 1987 with a Bachelor degree in Mechanical Engineering, she remained at the graduate school of University of Science and Technology of China in Modern Mechanics Department. In August, 1989, she married Yutong Wu. At the end of 1989, she came to the United States, and began her graduate study in Engineering Science and Mechanics Department at Virginia Polytechnic Institute and State University in February, 1990. After receiving her Master of Science degree in May, 1992, she will move to New Jersey to join her husband.

The author is a member of Adhesion Society and Society of Experimental Mechanics.